NASA-CR-172589
19850020629

NASA Contractor Report No. 172589

EVALUATION OF A FAULT TOLERANT SYSTEM FOR AN INTEGRATED AVIONICS SENSOR CONFIGURATION WITH TSRV FLIGHT DATA

Alper K. Caglayan and Pankaj M. Godiwala

CHARLES RIVER ANALYTICS INC.

CAMBRIDGE, MA 02138

CONTRACT NAS1-17719

JUNE 1985

National Aeronautics and
Space Administration

Langley Research Center
Hampton, Virginia 23665

TABLE OF CONTENTS

LIST OF TABLES

LIST OF FIGURES

1. INTRODUCTION

This Final Report presents the results of NASA Contract NAS1-17719 entitled "Evaluation of Fault Tolerant Concepts". The intent of this effort is to investigate the performance of FINDS (Fault Inferring Nonlinear Detection System) developed earlier and documented in [1] - [3] with the use of actual sensor flight data for the NASA ATOPS B-737 aircraft. This report summarizes the changes made in the FINDS algorithm to accommodate flight data, false alarm and failure detection performance of FINDS using the sensor flight data, and modifications made to the failure detection and isolation (FDI) algorithm in FINDS to improve false alarm and failure detection performance.

Earlier studies [1] - [3] were restricted to analyzing the performance of the developed FDI methodology on the digital simulation of the NASA ATOPS B-737 aircraft. Although the vehicle simulation was a nonlinear six-degree-of-freedom program incorporating sensor inaccuracies due to postulated misalignment, scale factor, noise, and constant bias errors, this simulation did not account for lever arm effects, structural modes, post filtering of the measurement data, and other errors such as time varying sensor biases. Therefore, the use of flight recorded data in the present study addresses these important performance issues under real modelling errors which will be important in an eventual flight test of the FINDS algorithm.

Summarizing the results obtained with the sensor flight data driven version of FINDS (hereafter referred to as the flight data emulation of FINDS), the vehicle state and normal operating bias estimation performance of the no-fail filter is found to be excellent based on an analysis of the no-fail filter residuals. In detecting and isolating sensor bias failures injected into the flight data, results show an excellent performance with detection speed considerably faster for measurement sensors such as MLS than for input sensors such as accelerometers. This is in agreement with our earlier simulation studies. Finally, the modifications made to the FINDS detector and decision algorithms in this study results in an improvement both in false alarm and failure detection performance.

The organization of the report is as follows:
Chapter 2 presents an analysis of the sensor flight data. In particular, various signal processing results performed on the sensor flight data to determine the sensor noise parameters and dropout conditions are presented. False alarm and failure detection performance of FINDS with flight recorded sensor data is presented in Chapter 3. This chapter also contains the modifications made to the basic FDI algorithm. Conclusions and recommendations are presented in the final chapter.

2. ANALYSIS OF FLIGHT DATA

In this chapter, we present various statistical analyses performed on the flight recorded data. These statistical analyses were made in order to determine the sensor error parameters such as bias levels and noise characteristics. These sensor error parameters are used in the design of the no-fail filter, detectors, and decision rule in the FINDS algorithm. The sensor error analyses results presented here are also used in the discussion of the estimation and failure detection performance in the next chapter. We begin this chapter with a description of the sensor measurements available on the flight data.

2.1 Flight Data Sensor Complement and Flight Path

Flight recorded data contains triple redundant outputs for flight control roll, pitch and yaw rate gyros; Inertial Measurement Unit (IMU) roll, pitch, and yaw attitudes; and indicated airspeed; dual redundant outputs are available for the flight control longitudinal, lateral and normal accelerometers and the radar altimeter measurements. On the other hand, only a single channel of data is available for the MLS azimuth, elevation and range measurements. Except for the body mounted rate gyro outputs, the third channel for the triple replicated sensors contained bad data. Hence, a dual redundant sensor complement is used for the FINDS exercise by simulating a dual channel for the MLS measurements.

The measurement data for the first replication of flight control accelerometers and rate gyros are given in Figures 2.1-3. These measurements depict the linear and angular accelerations sensed due to the aircraft maneuvers executed during the particular flight. For instance, the lateral accelerometer, and roll and yaw rate gyro outputs, show a bank maneuver around 100-140 seconds. Simularly, the longitudinal and lateral accelerometer, and pitch and yaw rate gyro outputs indicate a pitch-up and bank maneuver in the final phase (277-298 seconds) of the flight. We will refer to these figures in the discussion of the flight path correlated errors in the sensor flight data.

2.2 Determination of Replicated Sensor Error Parameters

The performance analysis of the developed fault tolerant system using flight data normally requires the determination of the sensor error parameters corresponding to the actual data. For the replicated measurements, one way of determining these parameters is to compute the difference between replicated sensor outputs, and to determine the sensor error characteristics from this difference signal. Consider the following representation for the two replicated sensor outputs y_1 and y_2:

$$y_1(k) = s(k) + c_1(k) + b_1 + v_1(k) \tag{2.1}$$

$$y_2(k) = s(k) + c_2(k) + b_2 + v_2(k) \tag{2.2}$$

where $s(k)$ is the true signal being measured, $c_i(k)$ is the sensor inaccuracy arising in both channels, for instance, from lever arm effects and structural modes in the case of body mounted instru-

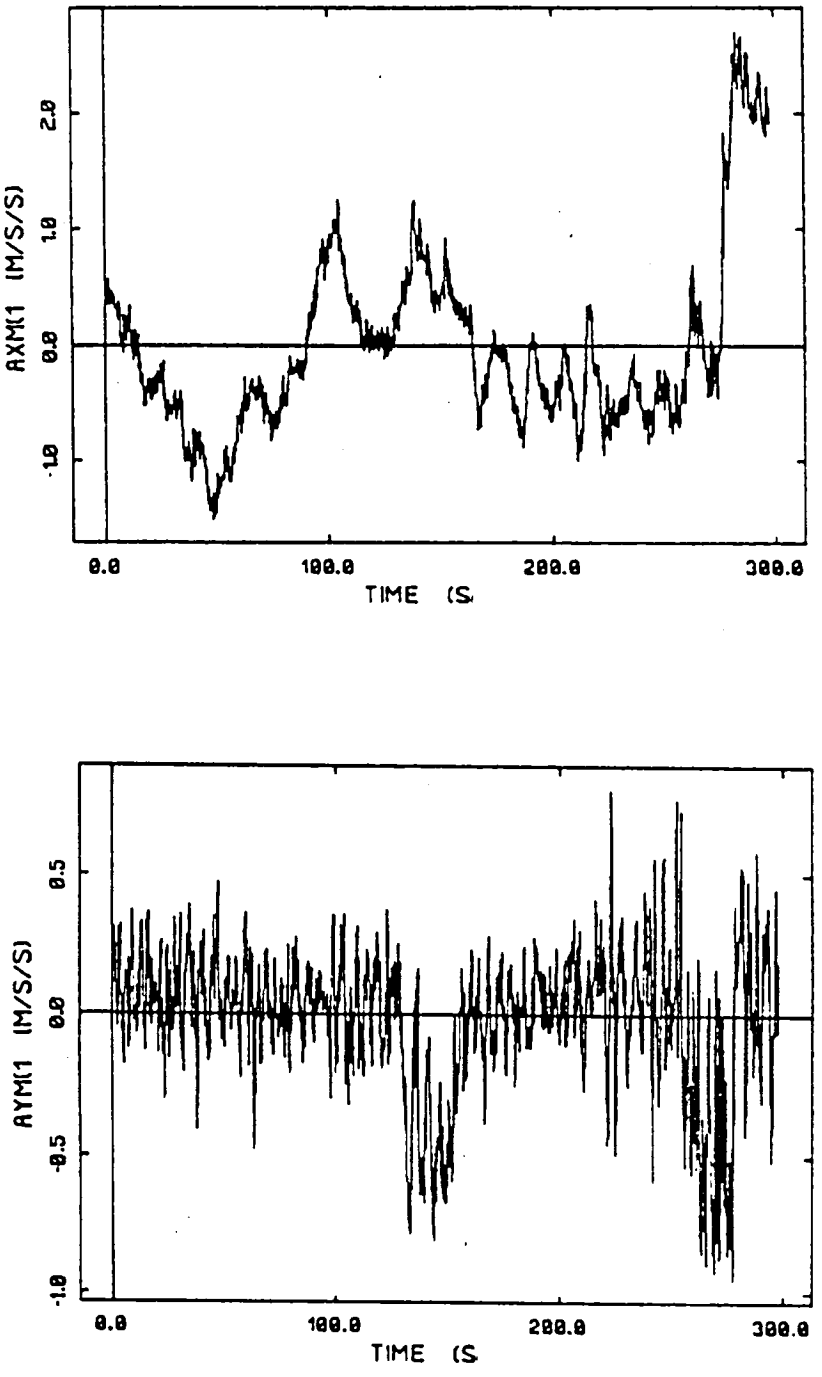

Figure 2.1: Longitudinal and lateral accelerometer sensor flight data time history

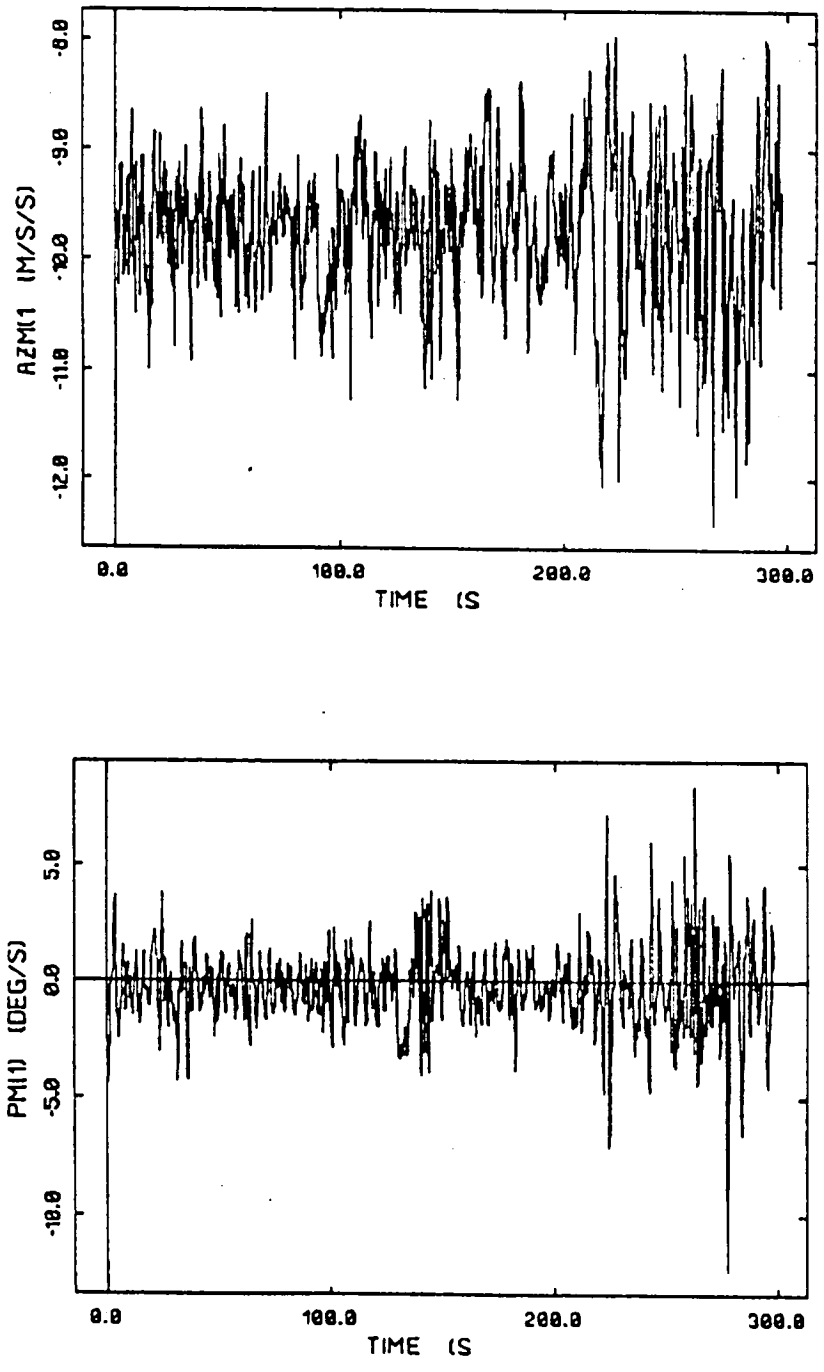

Figure 2.2: Normal accelerometer and roll rate gyro sensor flight data time history

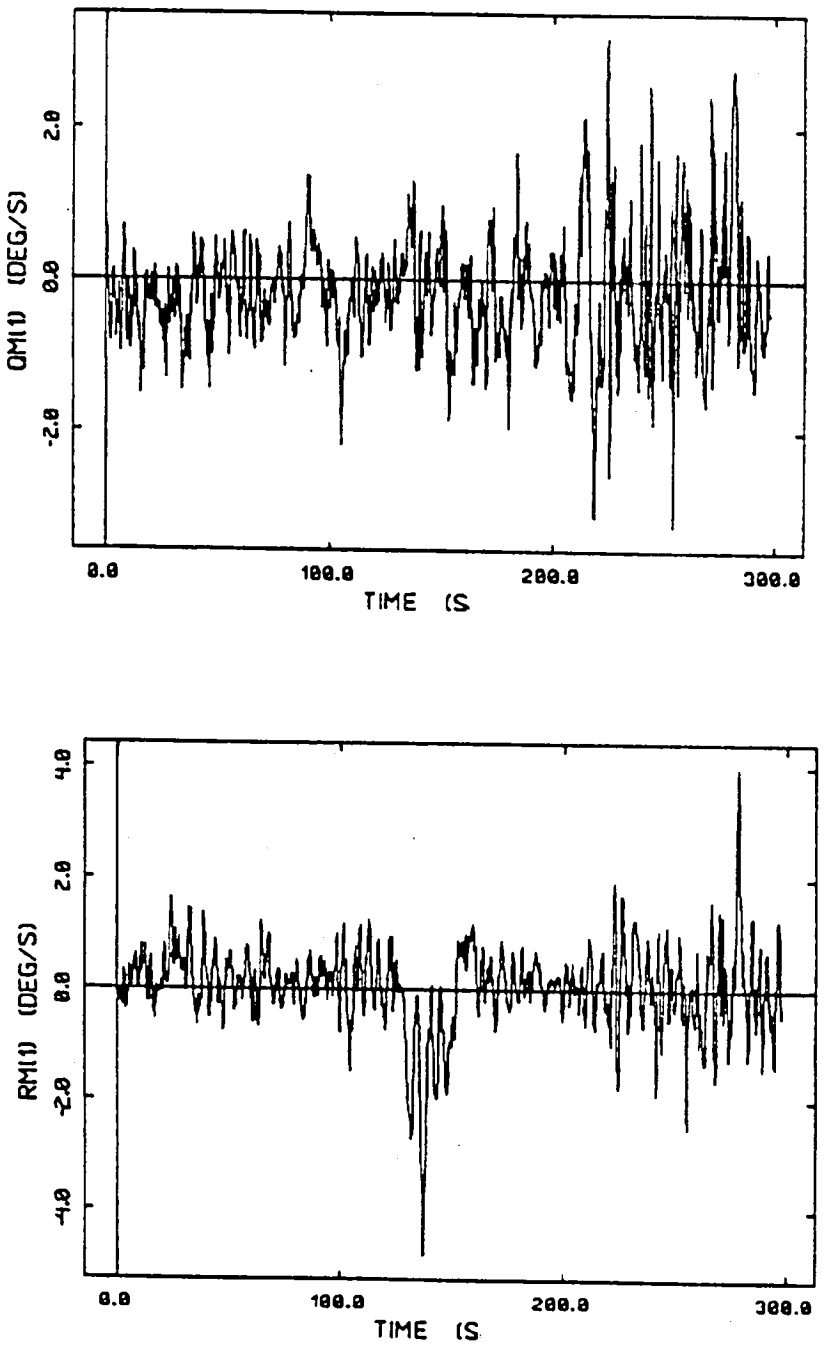

Figure 2.3: Pitch and yaw rate gyro sensor flight data time history

ments, b_1 and b_2 are the two normal operating bias levels associated with the two instruments, and $v_1(k)$ and $v_2(k)$ are two zero mean uncorrelated noise sequences with identical standard deviations. Forming the difference of the two measurements and normalizing with $\sqrt{2}$, we get as the difference signal

$$e_{12}(k) = (y_1(k) - y_2(k))/\sqrt{2} = c_{12}(k) + b_{12} + v_{12}(k) \qquad (2.3)$$

with

$$c_{12}(k) = (c_1(k) - c_2(k))/\sqrt{2} \; ; \quad b_{12} = (b_1 - b_2)/\sqrt{2} \qquad (2.4)$$

where $c_{12}(k)$ is the sensor inaccuracy reflected in the difference signal caused by physical location differences, b_{12} is the difference bias and $v_{12}(k)$ is a zero mean white noise sequence with standard deviation, equal to that of the noise in the original measurements y_1 and y_2. Note that, in this analysis, common errors contained in $c_1(k)$ and $c_2(k)$, would get washed out as well. Hence, it is not possible with this approach to determine sensor errors that are correlated among the replicated channels so that the preceeding error analysis is on the optimistic side. However, the sensor errors due to common lever arm effects and structural vibrations not reflected in the difference signal are usually negligible compared to the sensor bias and noise terms.

Our simulation studies [1-3] of FINDS have shown that time-correlated sensor errors have a significant impact on the false alarm performance of the FINDS failure detection algorithm. Hence, in this study, we have made a thorough analysis of the sensor errors in both the time and frequency domains in order to

determine the temporal error characteristics present in the sensor flight data. In particular, we have, first, constructed these sensor error (channel difference) signals from the flight data. Next, we have computed the sample mean and standard deviation, and empirical autocorrelation function for each of these sensor error sequences. Using the computed autocorrelation function, we have then performed a whiteness test on these error sequences. Finally, we have found the discrete Fourier transform (discrete power spectral density) of the normalized autocorrelation function to analyze the correlation in the error data.

The results of these statistical analyses performed on the accelerometer, rate gyro, IMU attitude, indicated airspeed, and radar altimeter measurements are presented in Table 2.1 and Figures 2.4-15. Table 2.1 shows the computed sample means and standard deviations. The top graph in each of the Figures 2.4-15 shows the plot of the sensor error in appropriate units against time. The lower graph in each of these figures depicts the discrete power spectral density for the error time history given above. The power spectral density is plotted in dB's (10 times the natural log of the magnitude of the discrete Fourier transform for the normalized autocorrelation function) against Hertz. The whiteness test results performed on the empirical autocorrelation function are given in Table 2.2.

Sensor Type	Computed Statistics		
	Sample Mean	Std. Dev.	Units
Longitudinal Accel.	-0.1980	0.0442	m/s/s
Lateral Accel.	0.0812	0.0532	m/s/s
Vertical Accel.	0.0652	0.1200	m/s/s
Roll Rate Gyro	-0.2640	0.0461	deg/s
Pitch Rate Gyro	-0.2140	0.0477	deg/s
Yaw Rate Gyro	0.1070	0.0310	deg/s
IAS	0.9100	0.2510	m/s
IMU Roll	0.0675	0.1110	deg
IMU Pitch	-0.1750	0.2610	deg
IMU Yaw	-0.0039	0.0891	deg
Radar Altimeter	-0.6215	0.2231	m

Table 2.1: Empirical statistics for sensor flight data channel differences

For the body mounted accelerometers, the computed sample means 0.1 - 0.2 m/s^2 have the same order of magnitude as that assumed in our previous studies [1] - [3] for accelerometer biases. Time histories for the accelerometer errors shown in Figure 2.4-6 show that the computed sample means correspond to essentially constant accelerometer biases. Similarly, the computed sample standard deviations of 0.05 - 0.1 m/s^2 are close to previously postulated accelerometer noise levels. As seen from Table 2.2, whiteness tests performed on the autocorrelation of accelerometer error sequences indicate that the accelerometer errors are time-correlated. This table also gives the percent of

Sensor Type	Autocorrelation Test Result	Percent Outside (2 s.d.)
Longitudinal Accel.	Correlated	16.00
Lateral Accel.	Correlated	33.33
Vertical Accel.	Correlated	8.33
Roll Rate Gyro	Correlated	69.67
Pitch Rate Gyro	Correlated	75.33
Yaw Rate Gyro	Correlated	37.00
MLS Azimuth *	Correlated	45.33
MLS Elevation *	Correlated	94.67
MLS Range *	Correlated	50.00
IAS	Correlated	72.67
IMU Roll	Correlated	92.67
IMU Pitch	Correlated	100.00
IMU Yaw	Correlated	81.33
Radar Altimeter	Correlated	87.67

*NOTE: Whiteness test was performed on MLS sensors using empirical error signals as replicated channels were not available.

Table 2.2: Whiteness test results for sensor flight data channel differences

times the sample autocorrelation lies outside 95% probability limits. As the table shows, the vertical and lateral accelerometers are, respectively, the least and most correlated accelerometer errors. The power spectral density for these sensor errors shown in Figures 2.4-6 indicate that the sensor inaccuracies, while not exactly white, have almost a constant power spectrum.

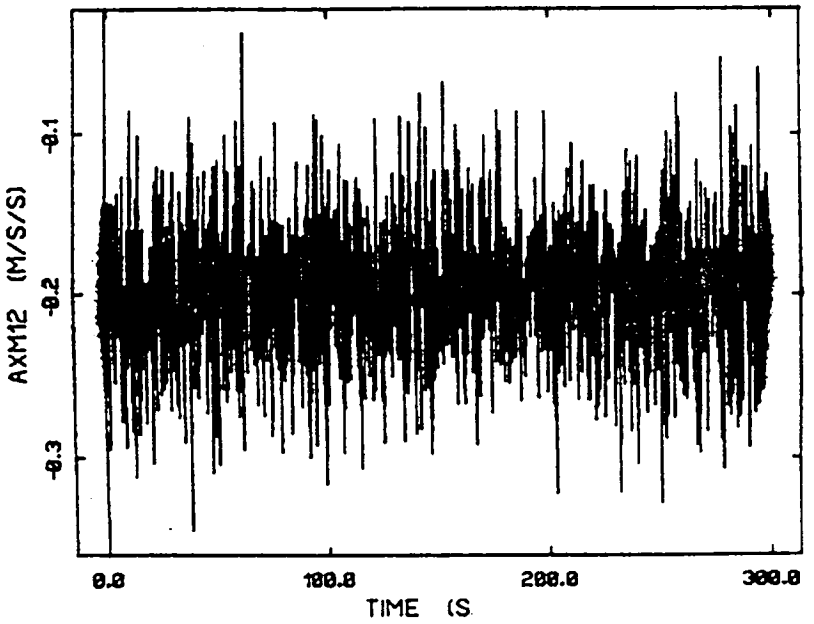

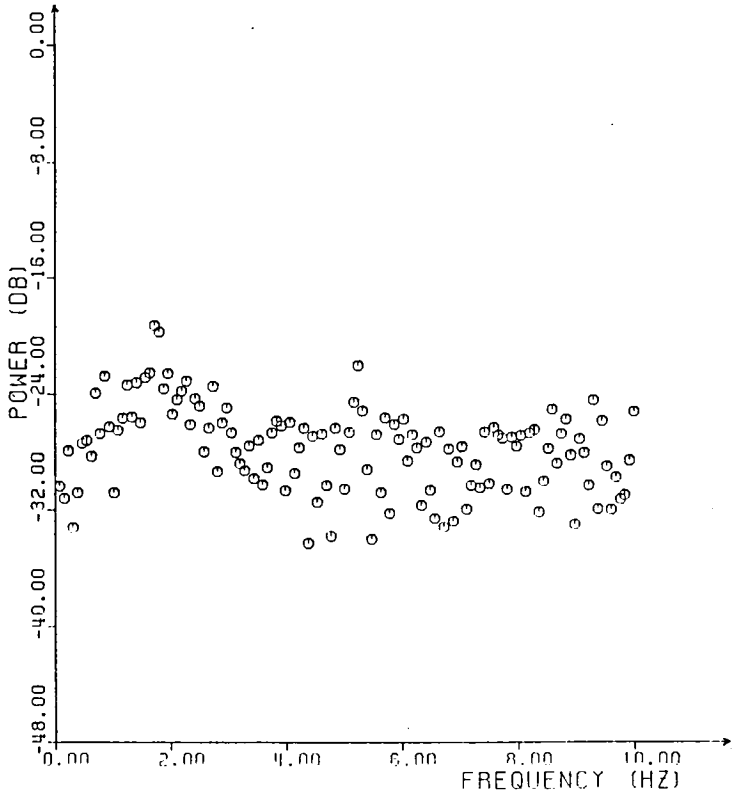

Figure 2.4: Time history and spectral density of longitudinal accelerometer error

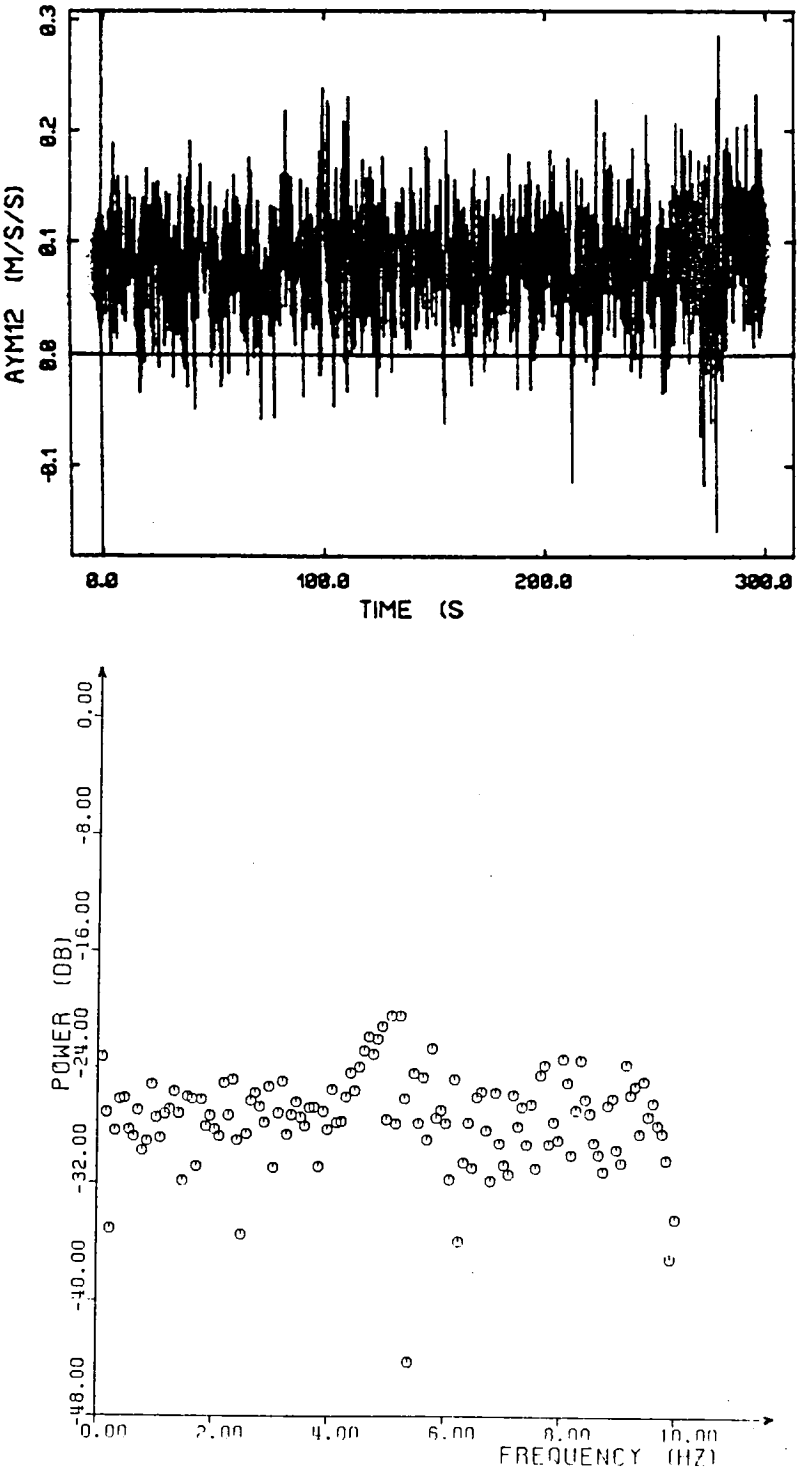

Figure 2.5: Time history and spectral density of lateral accelerometer error

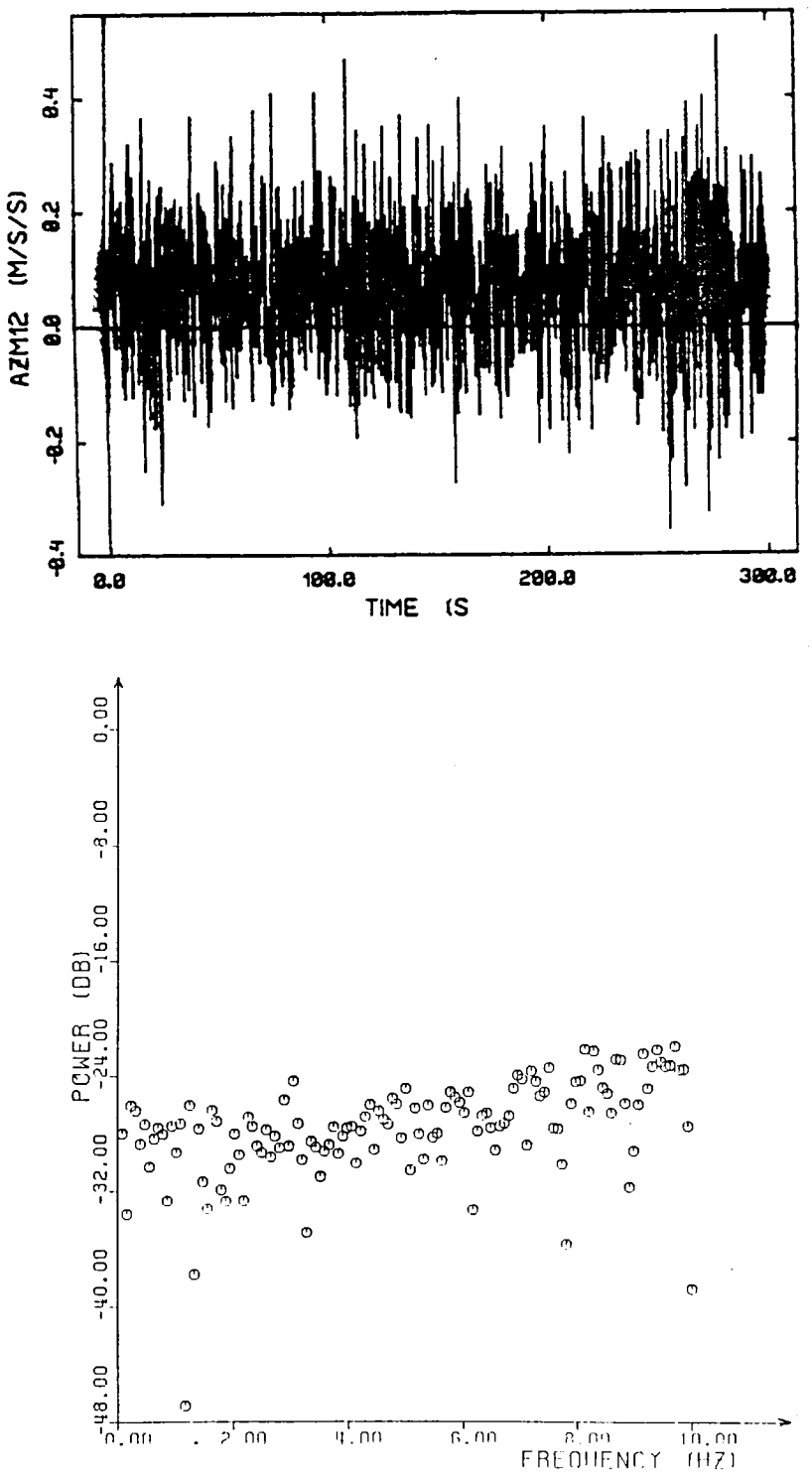

Figure 2.6: Time history and spectral density of vertical accelerometer error

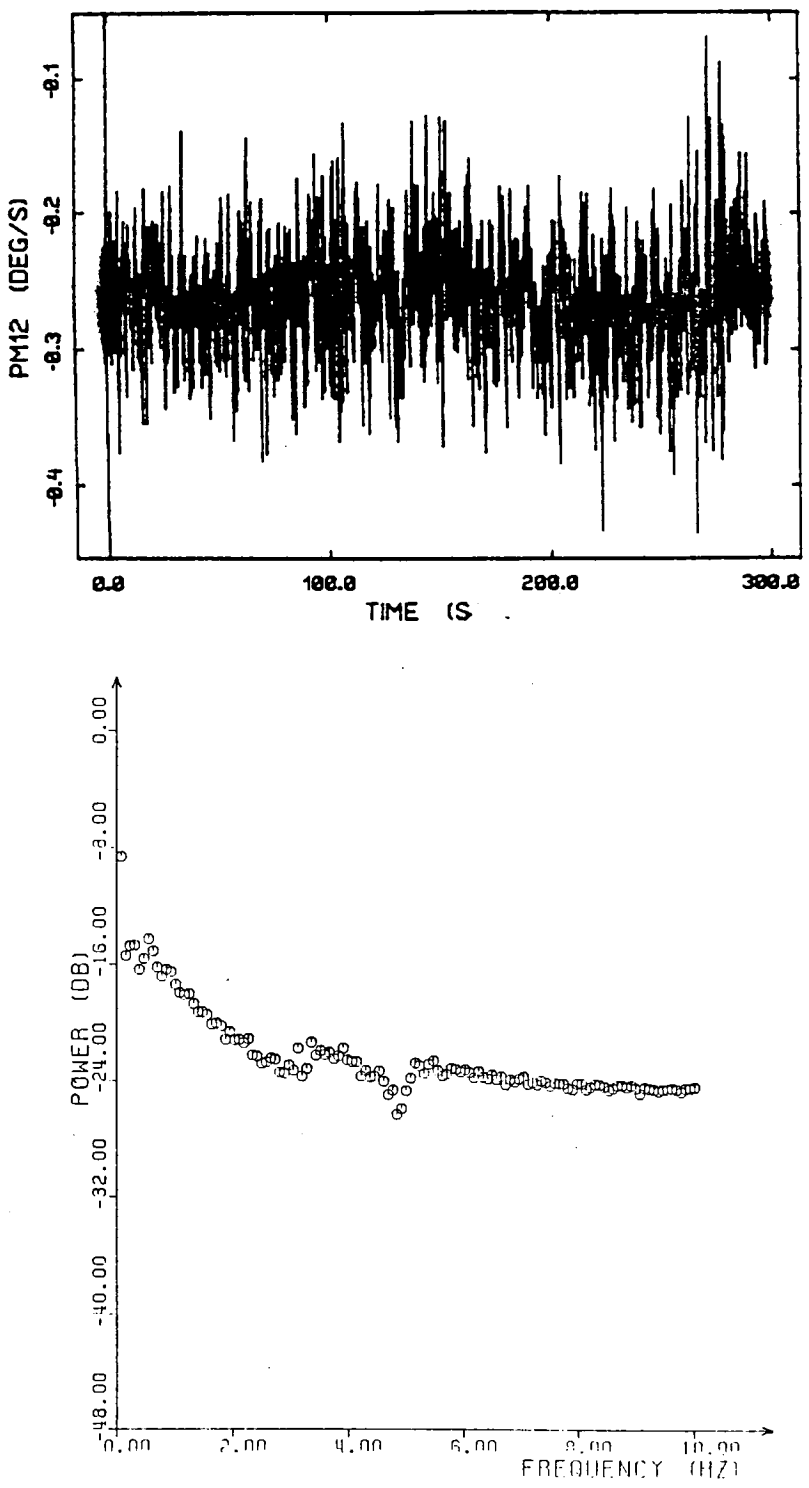

Figure 2.7: Time history and spectral density of roll rate gyro error

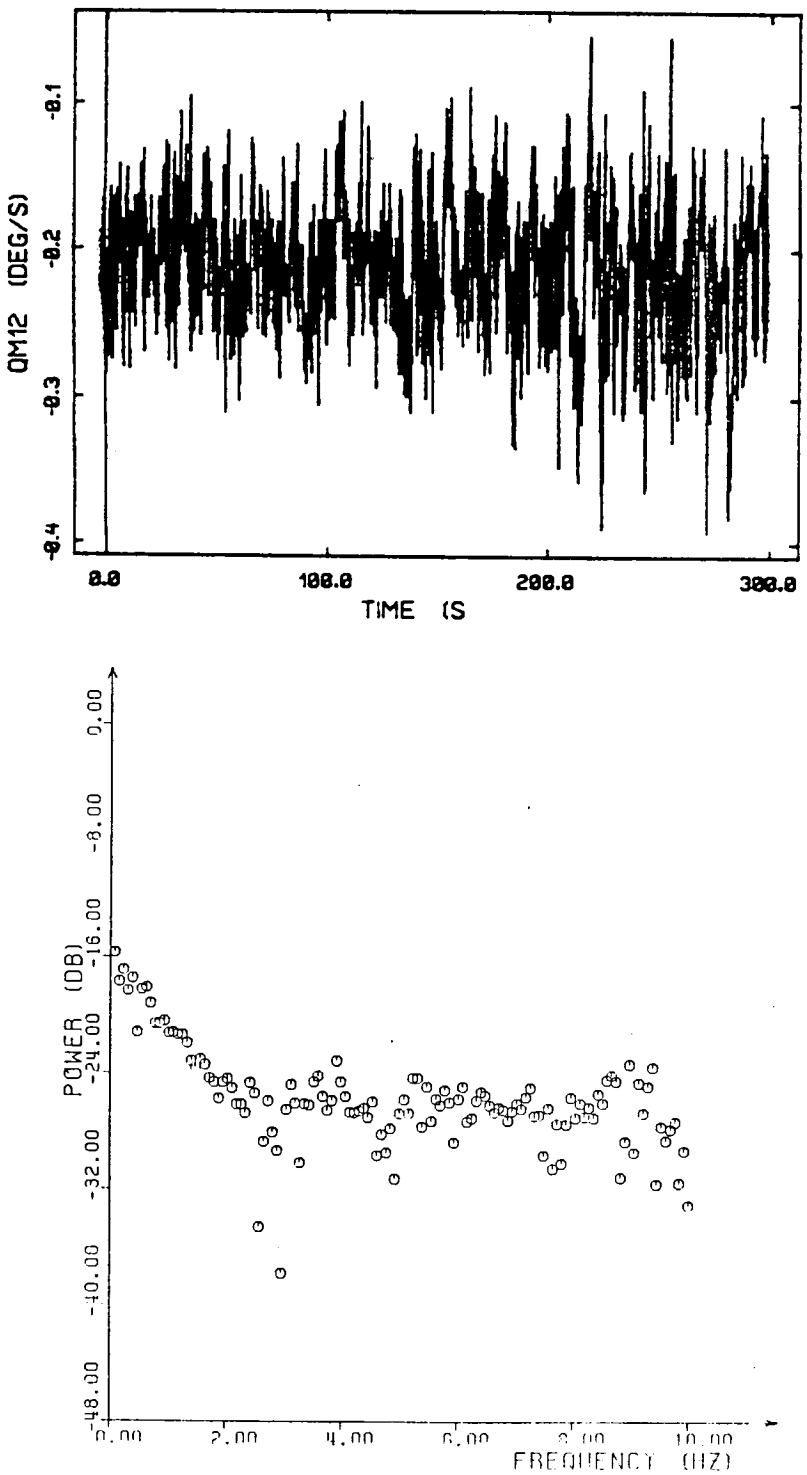

Figure 2.8: Time history and spectral density of pitch rate gyro error

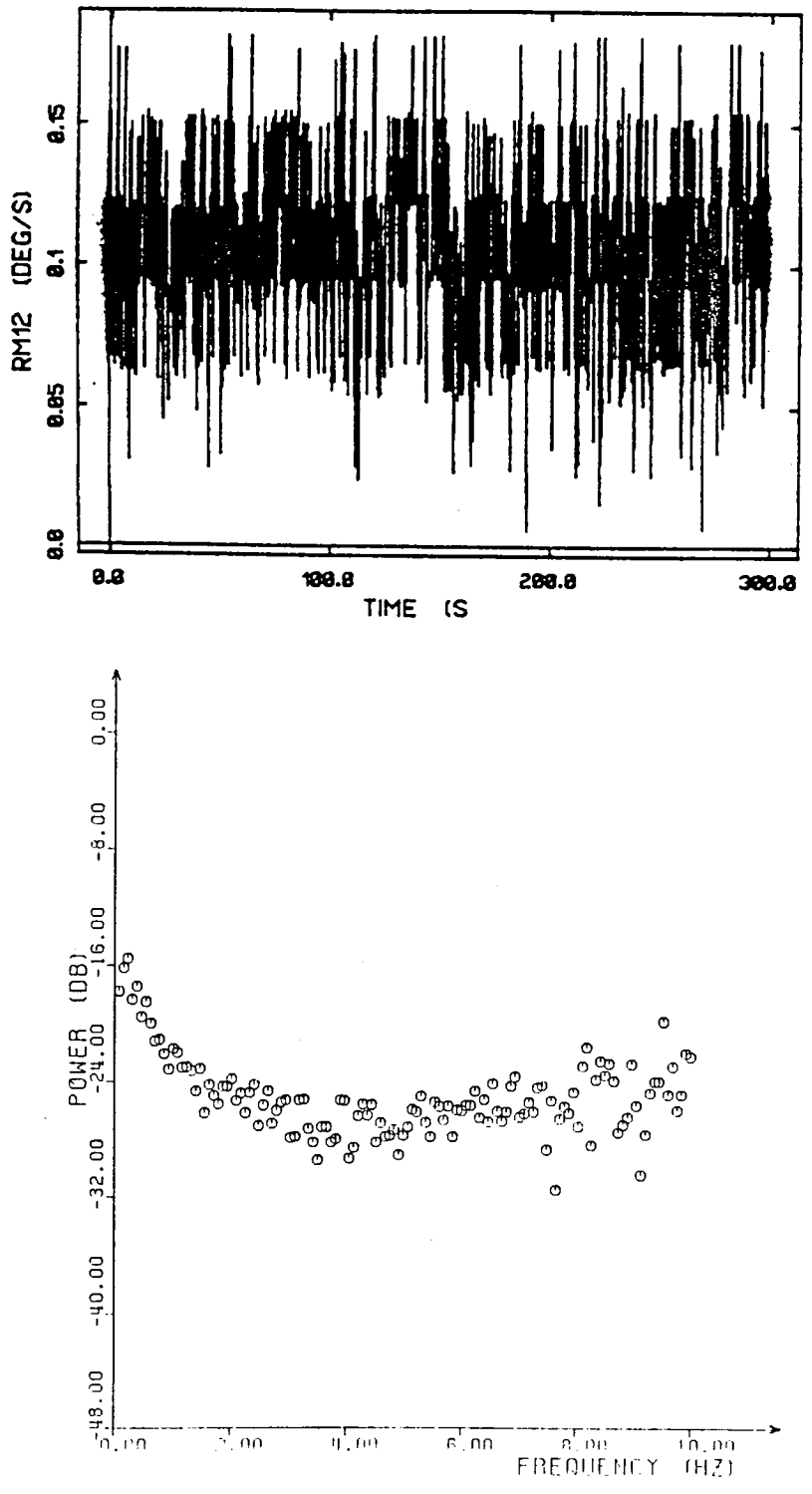

Figure 2.9: Time history and spectral density of yaw rate gyro error

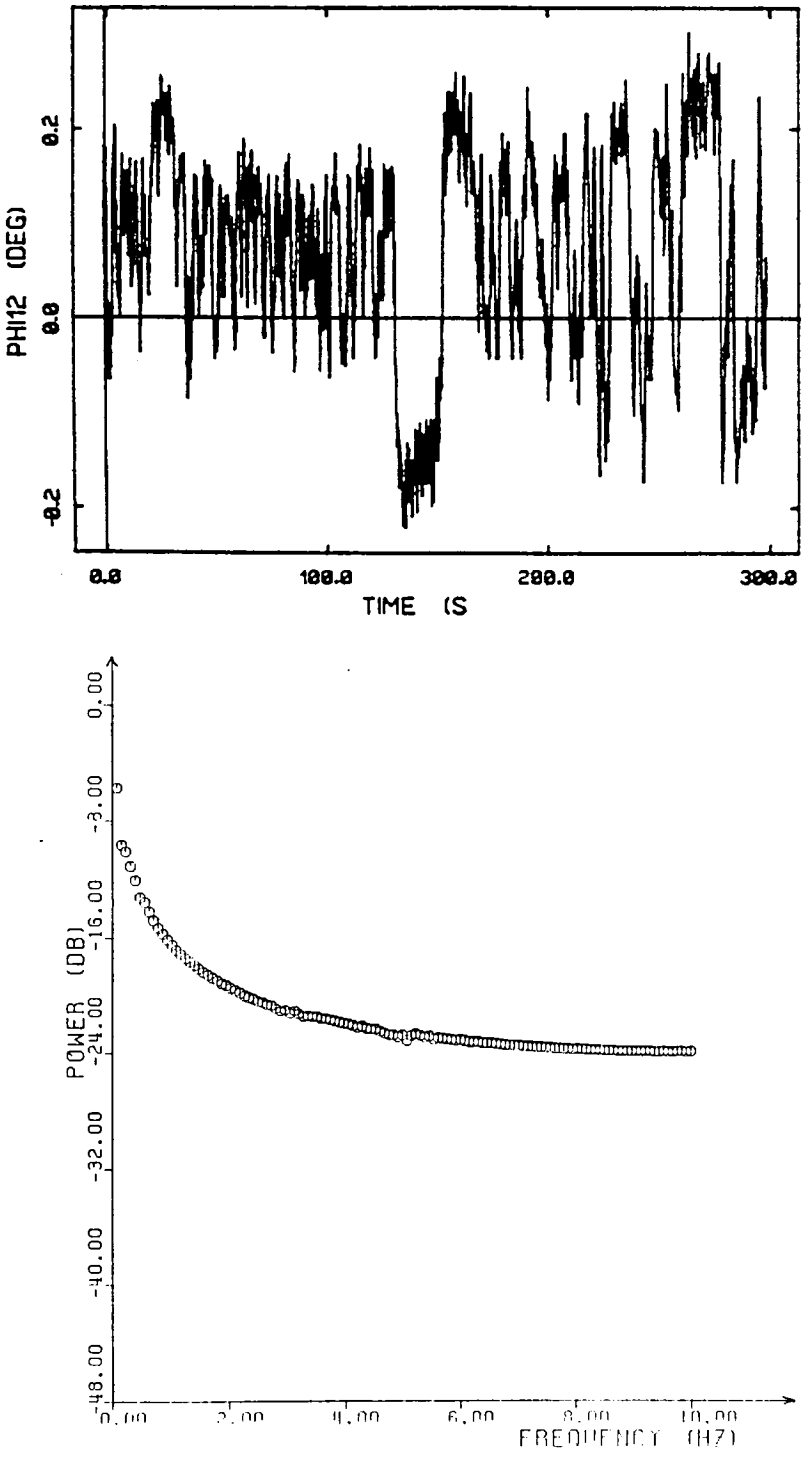

Figure 2.10: Time history and spectral density of roll attitude error

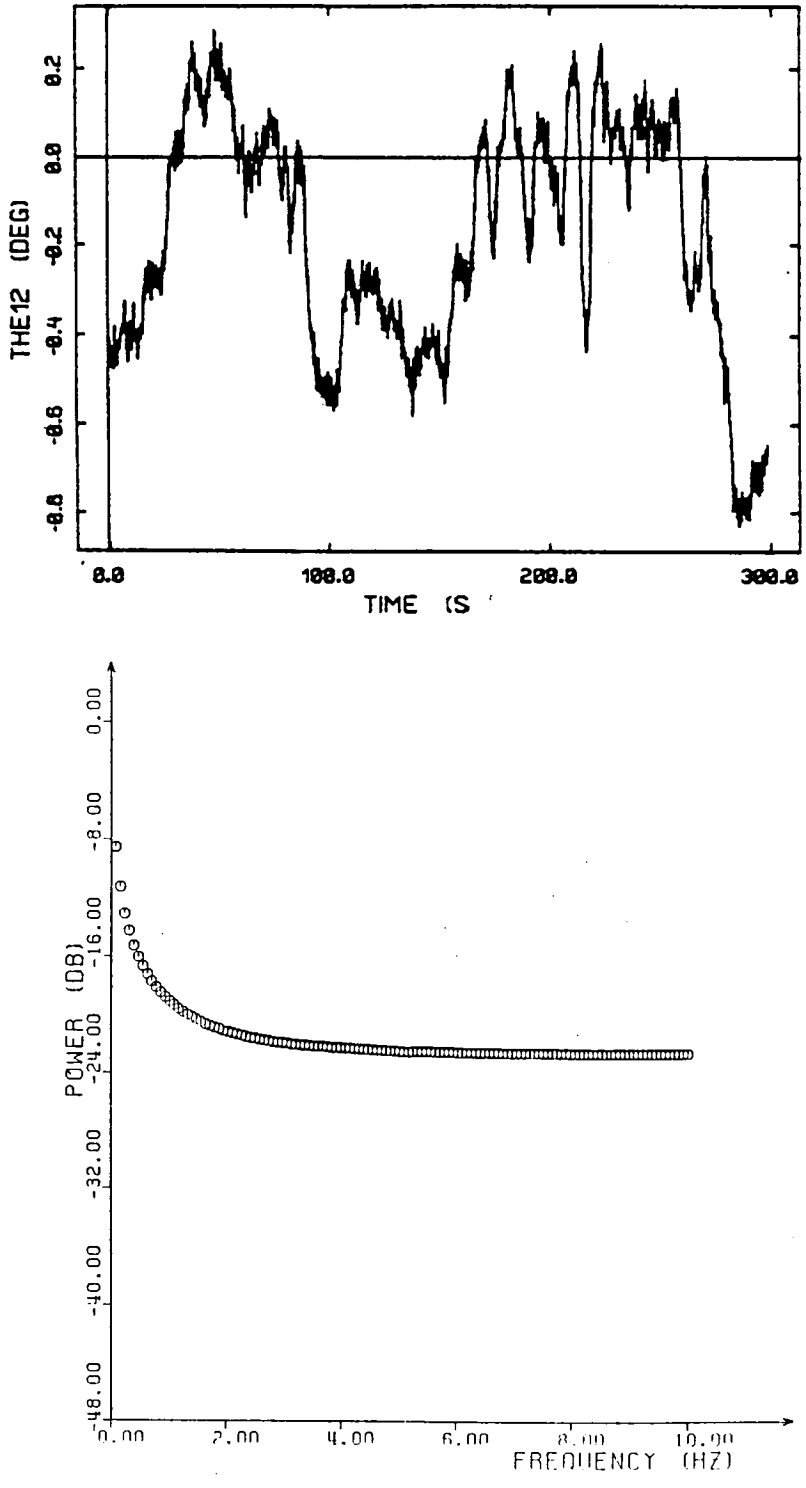

Figure 2.11: Time history and spectral density of pitch attitude error

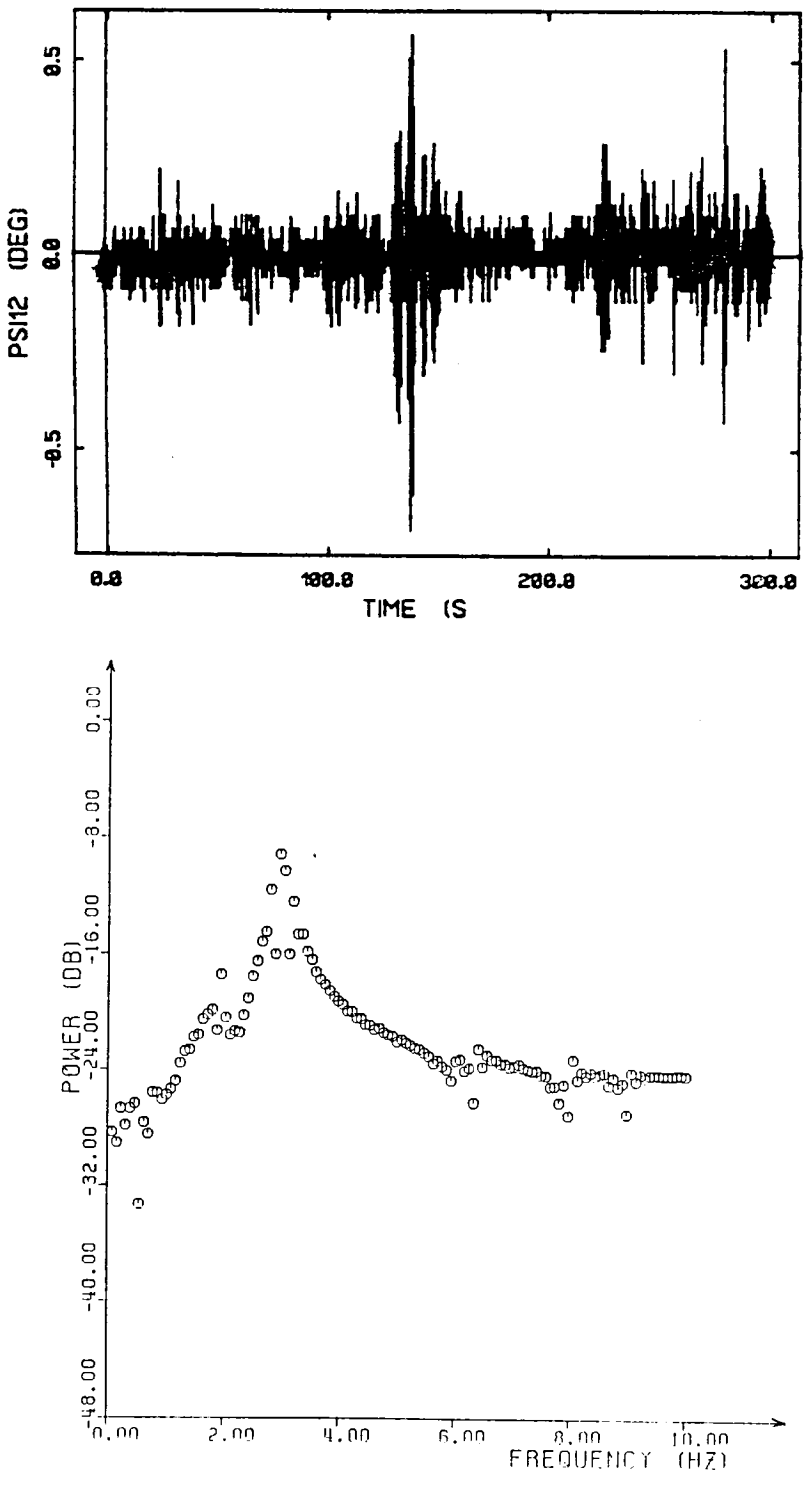

Figure 2.12: Time history and spectral density of yaw attitude error

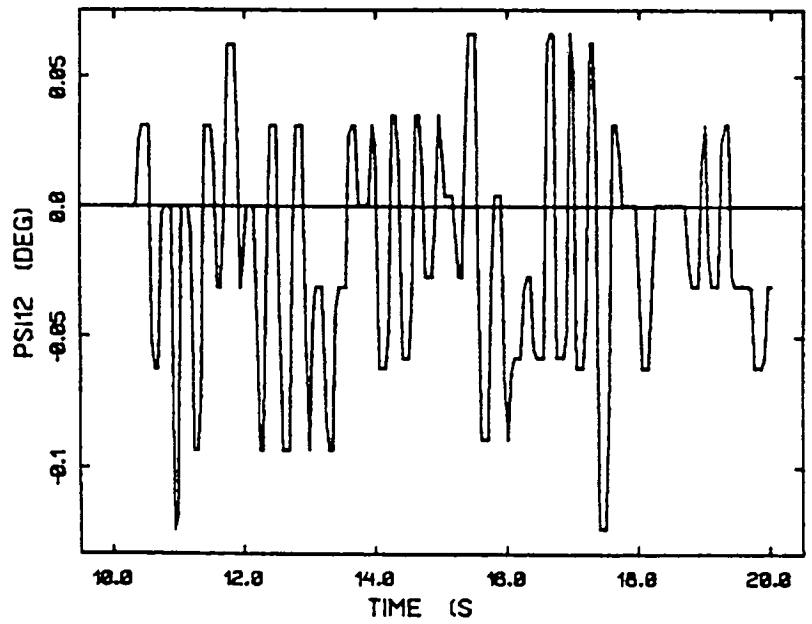

Figure 2.13: Expanded time history of yaw attitude error

The computed sample means of 0.1 - 0.25 deg/s for the body mounted rate gyro difference signals are significantly higher than the rate gyro bias levels assumed in our previous work [3], while the computed sample standard deviations of 0.03 - 0.05 deg/s are slightly larger than noise levels assumed in our previous simulations. As can be seen from the plots of rate gyro difference signals in Figures 2.7-9, rate gyros have varying

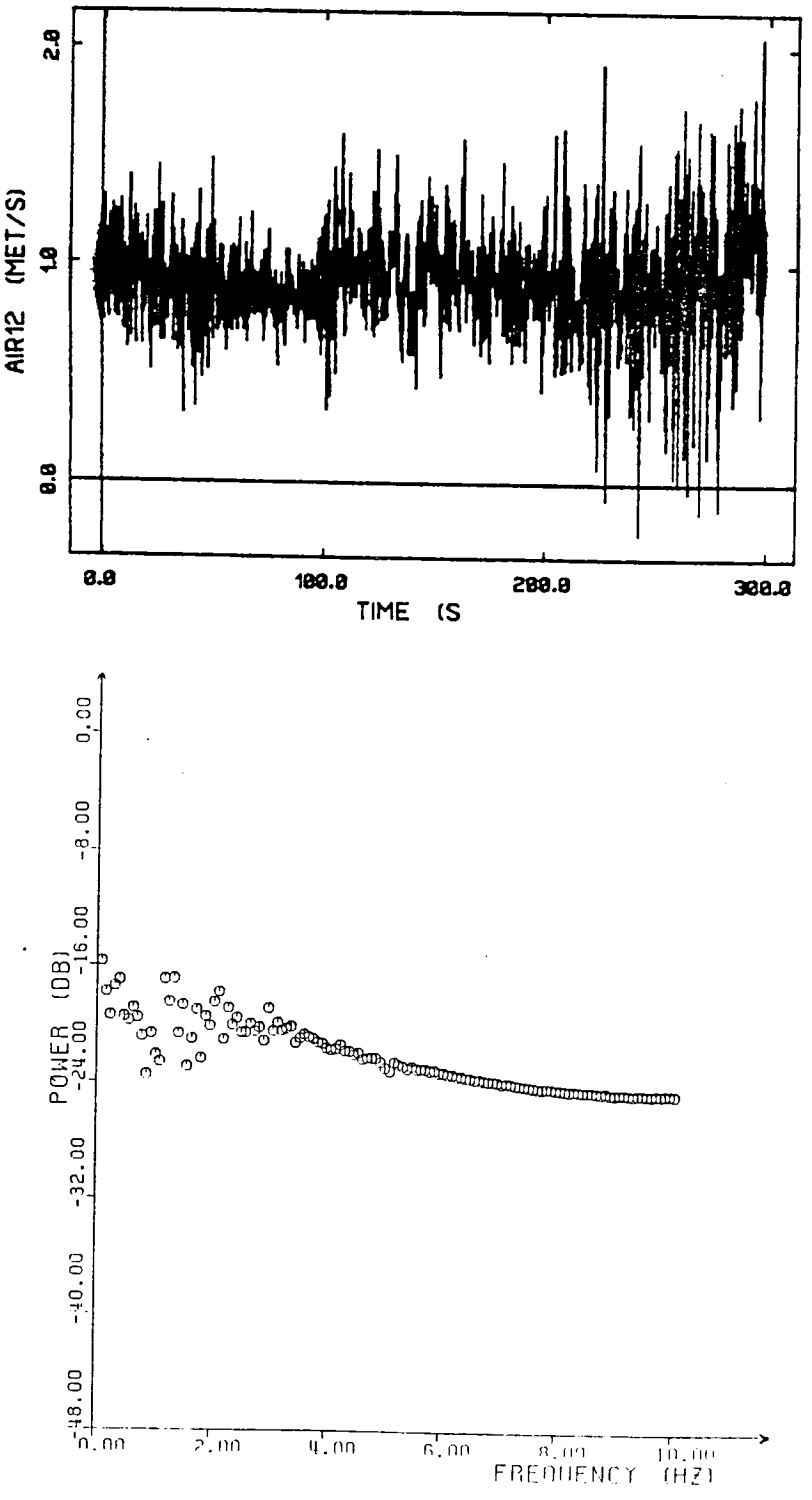

Figure 2.14: Time history and spectral density of indicated airspeed error

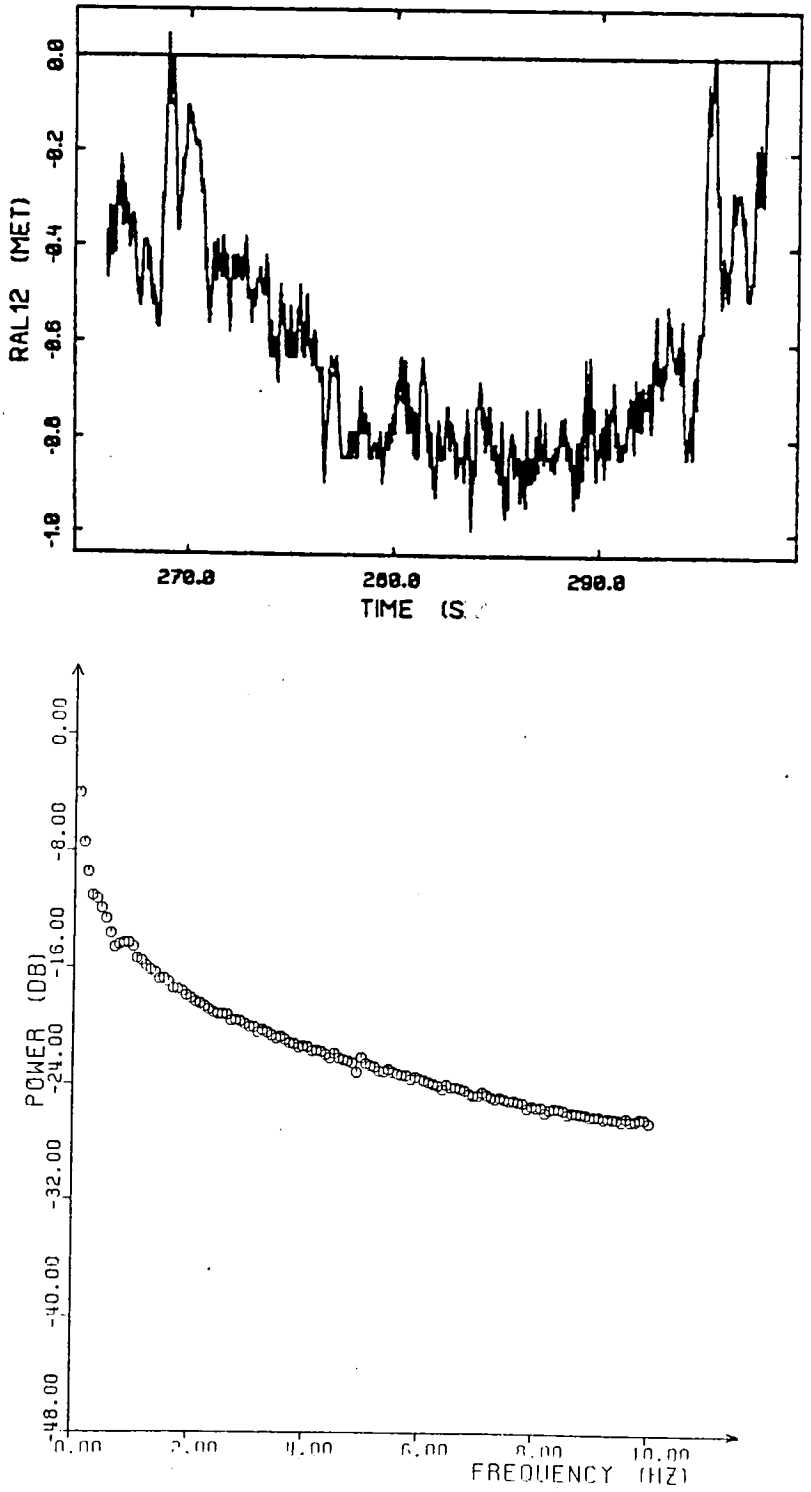

Figure 2.15: Time history and spectral density of radar altimeter error

biases due to scale factor and misalignment errors during maneuvers. The dependence of rate gyro errors on the flight path can be seen by comparing these error time histories with those for the rate gyro measurements depicted in Figure 2.2-3. Note, for instance, the roll rate gyro degradation at around 100 seconds. Also note that the yaw rate gyro exhibits quantization errors. Power spectral density for the rate gyro errors shown in Figures 2.7-9 indicate that the constant density property of a temporally uncorrelated error sequence is most seriously violated at low frequencies. Time correlation in these error signals is also evident from tests of whiteness given in Table 2.1.

For the attitude measurements, the computed sample means of 0.02 - 0.2 degrees and sample standard deviations of 0.09 - 0.25 degrees have the same order of magnitude as the attitude sensor bias and noise levels postulated in our simulations. The time histories for the attitude sensor difference signals are depicted in Figures 2.10-12 which show an irregular variation of the bias levels for these instruments with time, mostly due to maneuvers. In the case of yaw attitude sensor, note the substantial accuracy degradation during the flight segment between 130-150 seconds during the bank maneuver indicated by the yaw rate gyro measurement output in Figure 2.3. An expanded time history of the yaw attitude sensor difference is presented in Figure 2.10 which depicts an almost square-wave error with a 3 Hz frequency. This

characteristic is also evident from the peak at 3 Hz in the power spectral density of the yaw attitude error depicted in Figure 2.12. In contrast, the power spectral density for the IMU roll and pitch attitudes exhibit deviation from whiteness at low frequencies. Tests of whiteness for the IMU attitude sensors given in Table 2.2 verify the extreme time correlation present in these error signals.

The computed sample mean of 1.0 m/s and standard deviation of 0.2 m/s for the indicated airspeed are within the previously assumed ranges for the IAS bias and noise levels. Figure 2.14 contains the time history for the IAS sensor difference signal which shows a nearly constant bias but a higher noise level near touchdown. Power spectral density of the IAS error indicates an uncorrelated behavior at frequencies over 3 Hz.

For the radar altimeter, the computed sample mean of 0.6 and standard deviation of 0.25 meters are again within the postulated ranges for the radar altimeter bias and noise levels. Time history for the radar altimeter difference signal shown in Figure 2.15 shows that the bias levels are time varying. Power spectral density and whiteness test results verify the time correlation observed in the time history.

2.3 MLS Sensor Error Characteristics

Since only one channel of MLS azimuth, elevation and range sensor data was available, the statistical error analysis of the

previous section could not be used on these measurements. For the MLS sensors, we have made a linear least squares fit over a moving window of five measurements in order to compute the sensor errors. Table 2.3 shows the sample mean and standard deviations computed for these error sequences obtained.

As can be seen from the table, all of the MLS channels have negligible bias levels. The computed standard deviation of 0.003 deg for azimuth and elevation, and 0.5 meters for range are lower than the previously assumed noise levels.

Time histories for the MLS errors are shown in Figures 2.16-18. These error time histories do not show an obvious time-correlation in the MLS sensors. Since time-correlated MLS sensor errors had a significant impact on the false alarm performance of the FINDS algorithm, we have computed the MLS sensor-error time correlation empirically from the generated error sequences. As discussed in [4], the MLS noise sequences are time correlated and generated via:

$$v(k+1) = a\, v(k) + n(k) \tag{2.5}$$

where $n(k)$ is a zero mean white noise sequence, $v(k)$ is the colored MLS noise corrupting the measurement, and the scalar "a" is the correlation constant to be found. We have computed this constant by rearranging eqn. (2.5) as:

$$\begin{bmatrix} v(k) \\ v(k-1) \\ \cdot \\ \cdot \\ \cdot \\ v(2) \end{bmatrix} = \begin{bmatrix} v(k-1) \\ v(k-2) \\ \cdot \\ \cdot \\ \cdot \\ v(1) \end{bmatrix} a + \begin{bmatrix} n(k-1) \\ n(k-2) \\ \cdot \\ \cdot \\ \cdot \\ n(1) \end{bmatrix} \tag{2.6}$$

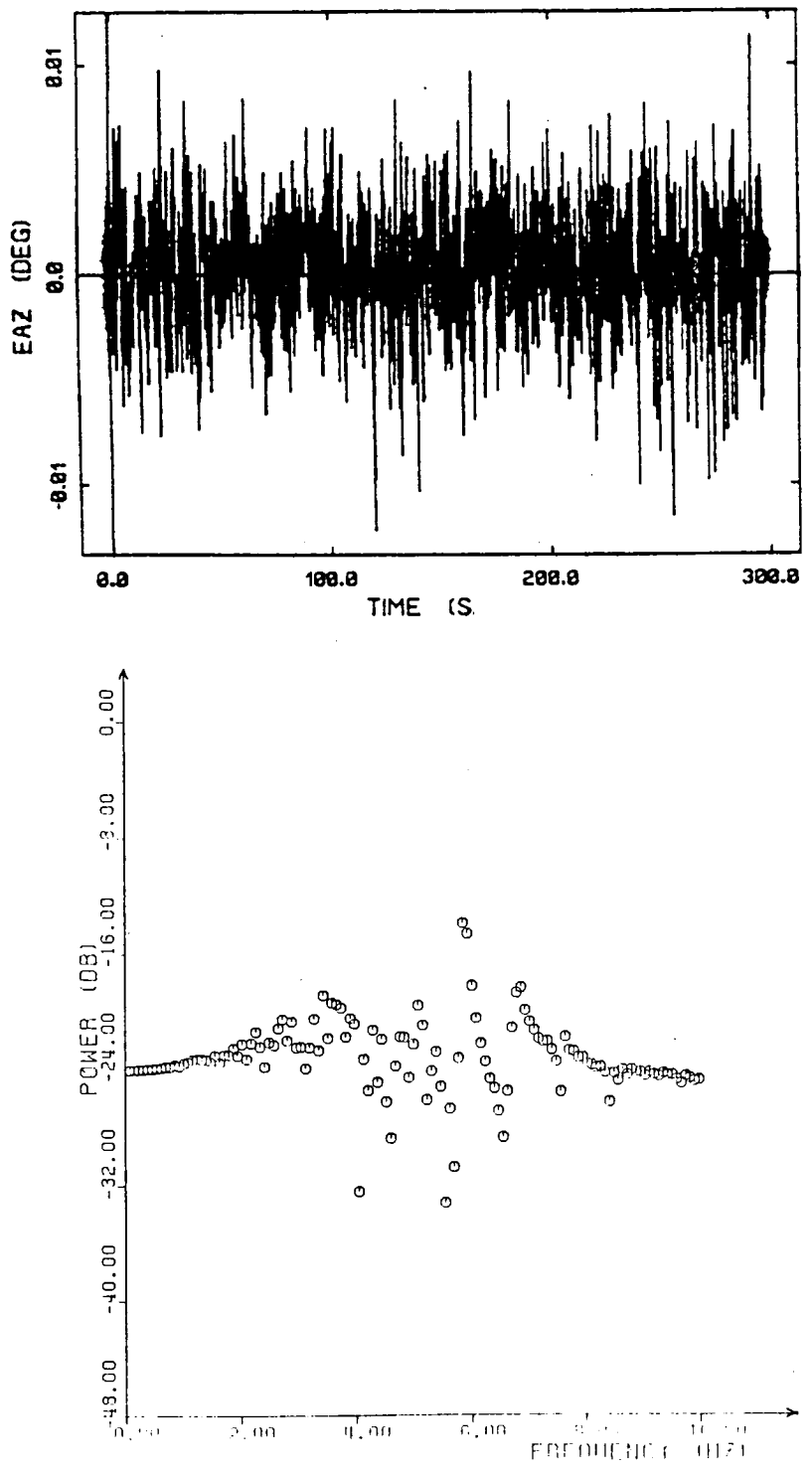

Figure 2.16: Time history and power spectral density of MLS azimuth error

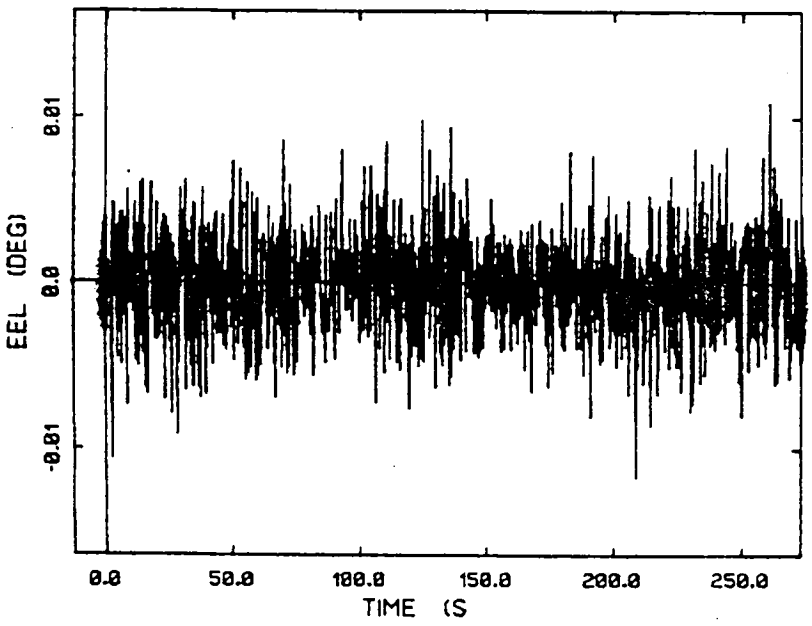

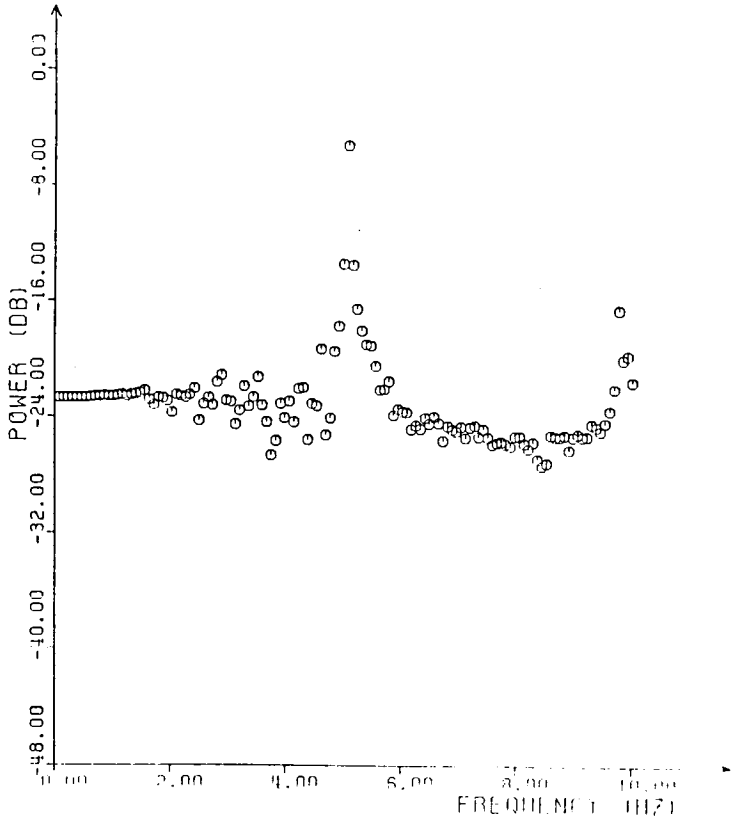

Figure 2.17: Time history and power spectral density of MLS elevation error

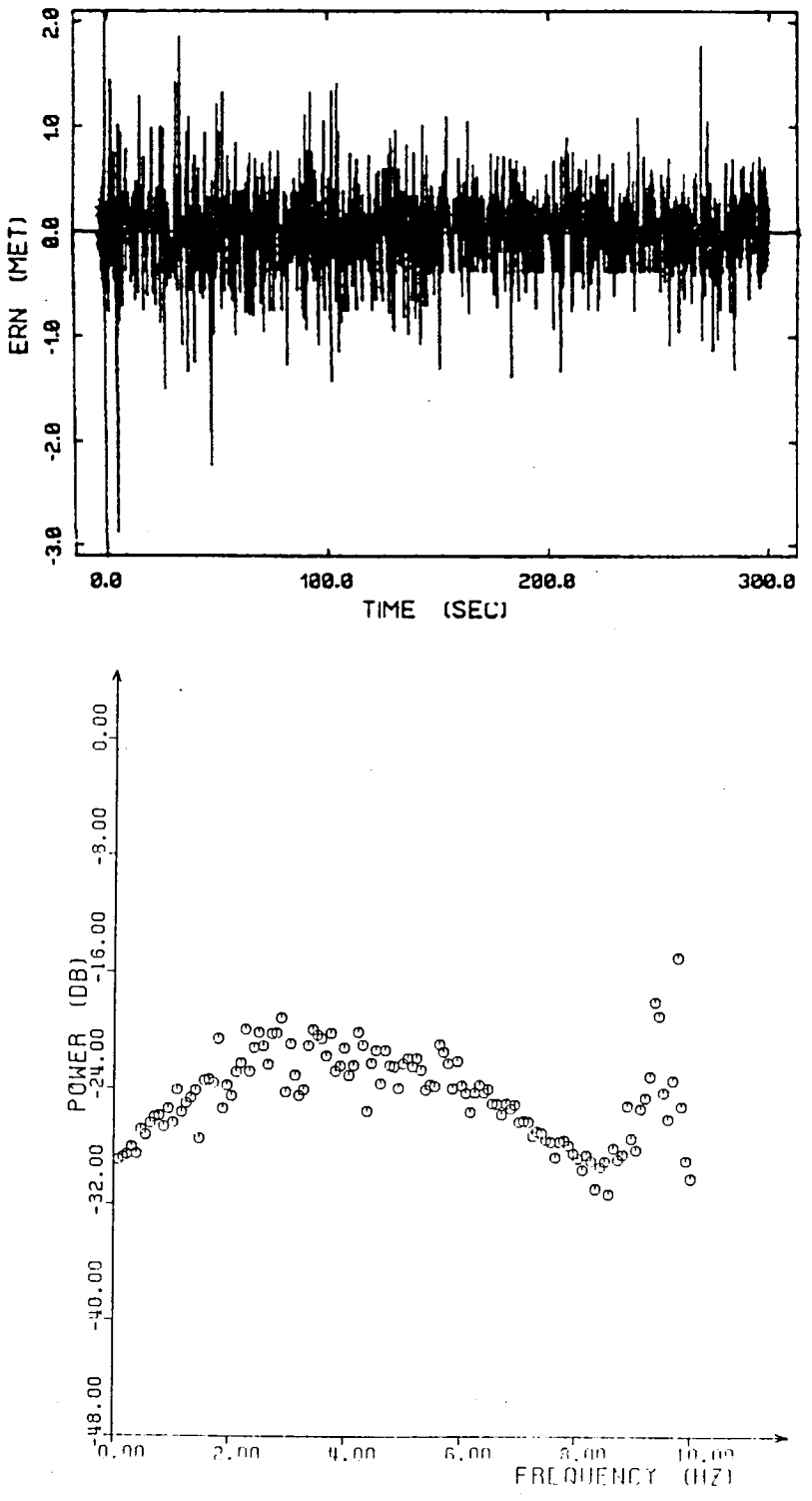

Figure 2.18: Time history and power spectral density of MLS range error

Sensor Type	Computed Statistics Sample Mean	Std. Dev.	Units
MLS Azimuth	0.665E-05	0.00312	deg
MLS Elevation	-0.360E-06	0.00316	deg
MLS Range	0.00266	0.483	m

Table 2.3: Empirical error statistics for MLS sensor flight data

The least squares estimate, $\hat{a}$, for the time correlation constant, a, is then given by:

$$\hat{a} = \sum_{j=1}^{k-1} v(j)v(j+1) \Big/ \sum_{j=1}^{k-1} v^2(j) \qquad (2.7)$$

The computed correlation constants were approximately 0.1, 0.3 and 0.2 for the azimuth, elevation, and range sensors. These values correspond to time constants of approximately 0.025, 0.05, and 0.034 seconds which are an order of magnitude smaller than the values used in our simulation studies (e.g. compared to 0.34, 0.25, 0.34 second time constants). These time constants estimates $\hat{\alpha}$, were computed according to:

$$\hat{\alpha} = -T \ln(\hat{a}) \qquad (2.8)$$

where T=0.05 s is the sampling interval. These computed time constants are not large enough to have an impact on the false alarm performance of the FINDS algorithm. The implications of this analysis will be discussed in the next chapter.

Whiteness tests performed on the MLS error sequences indicate the existence of time correlation in these errors. Power spectral density for the error sequences given in Figures 2.16-18 indicate the presence of a 5Hz peak in the elevation and 9Hz peak in the range error.

2.4 Reasonableness Tests and Data Dropouts

An analysis of the rate of change between two successive sampling instants were also made to ascertain the reasonableness of the data and to find out data dropout conditions. The results of this analysis are presented in Table 2.4. Again, using the following measurement model

$$y(k) = s(k) + v(k) \tag{2.9}$$

where s(k) is the true signal measured by the sensor and v(k) is the zero mean white measurement noise, then temporal difference will be given by:

$$y(k+1) - y(k) = s(k+1) - s(k) + v(k+1) - v(k) \tag{2.10}$$

Therefore, this difference signal will contain a white noise component with standard deviation two times that for the original measurement noise. Based on the expected time rate of change, and measurement noise statistics, we have set thresholds to identify dropout conditions. Table 2.4 summarizes these dropouts encountered in the flight data.

Sensor output time histories depicting the data dropout conditions are shown in Figures 2.19-22. For instance, MLS

elevation sensor data dropout at 212 seconds can be observed in Figure 2.21. Simularly, Figure 2.22 shows a simultaneous dropout in the two yaw attitudes around 277 seconds. Modifications have been made to the FINDS software to compensate for these detected dropout conditions.

Sensor Type	Rep.	Time(s)	Difference	
MLS Elevation	1	212.000	.723	deg
MLS Elevation	2	212.000	.723	deg
MLS Elevation	1	212.050	2.800	deg
MLS Elevation	2	212.050	2.800	deg
MLS Range	1	212.000	1396.280	m
MLS Range	2	212.000	1396.280	m
MLS Range	1	212.050	5397.937	m
MLS Range	2	212.050	5397.937	m
MLS Range	1	276.650	1107.983	m
MLS Range	2	276.650	1107.983	m
MLS Range	1	276.700	2135.339	m
MLS Range	2	276.700	2135.339	m
MLS Range	1	276.750	958.789	m
MLS Range	2	276.750	958.789	m
MLS Azimuth	1	276.700	.113	deg
MLS Azimuth	2	276.700	.113	deg
MLS Azimuth	1	276.750	.098	deg
MLS Azimuth	2	276.750	.098	deg
IMU Yaw	1	276.650	87.958	deg
IMU Yaw	2	276.650	87.964	deg
IMU Yaw	1	276.700	147.907	deg
IMU Yaw	2	276.700	147.918	deg
IMU Yaw	1	276.750	54.717	deg
IMU Yaw	2	276.750	147.918	deg
IMU Yaw	2	276.800	147.918	deg
IMU Yaw	2	276.850	147.918	deg
IMU Yaw	2	276.900	147.918	deg
IMU Yaw	2	276.950	44.468	deg
Vertical Accel.	2	277.600	1.375	m/s/s

Table 2.4: Sensor flight data dropouts

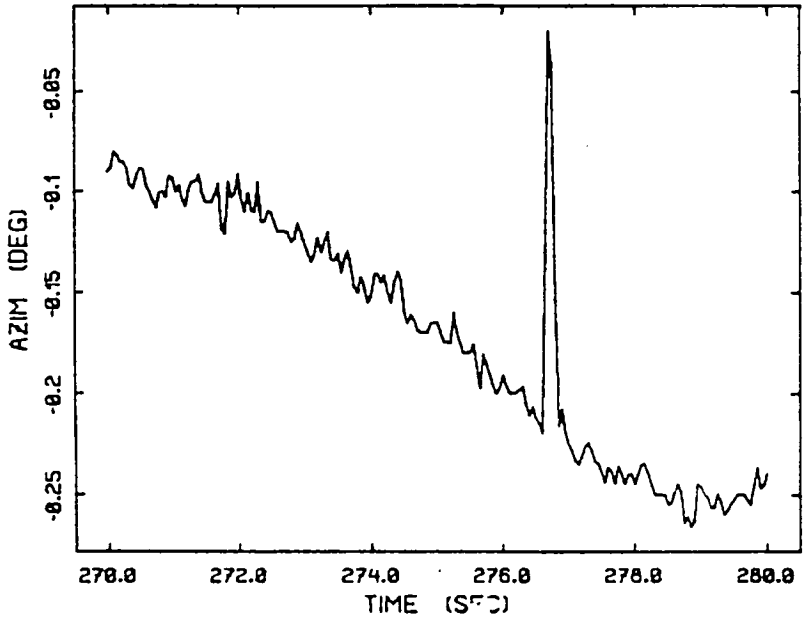

Figure 2.19: MLS azimuth dropout at 276.65 seconds

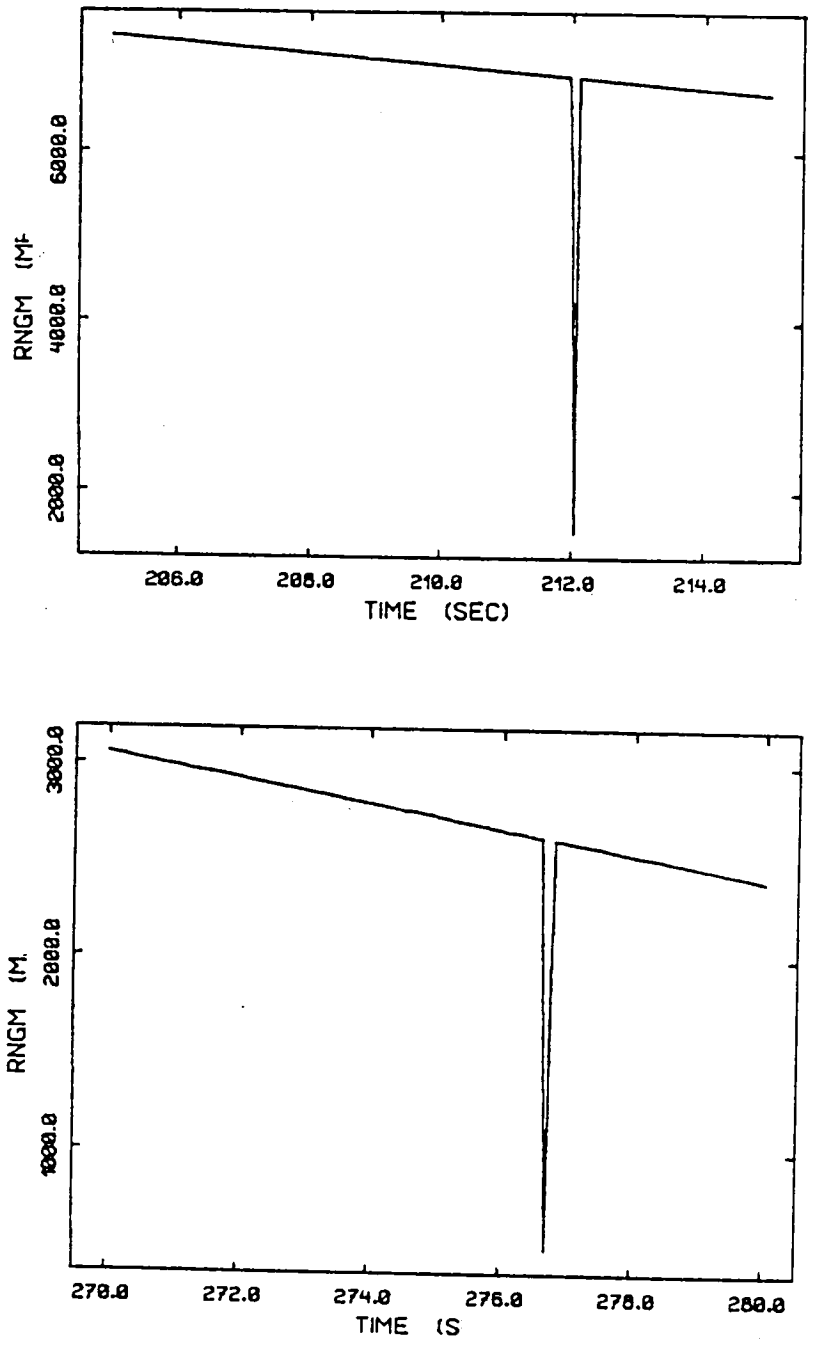

Figure 2.20: MLS range dropouts at 212 and 276.65 seconds

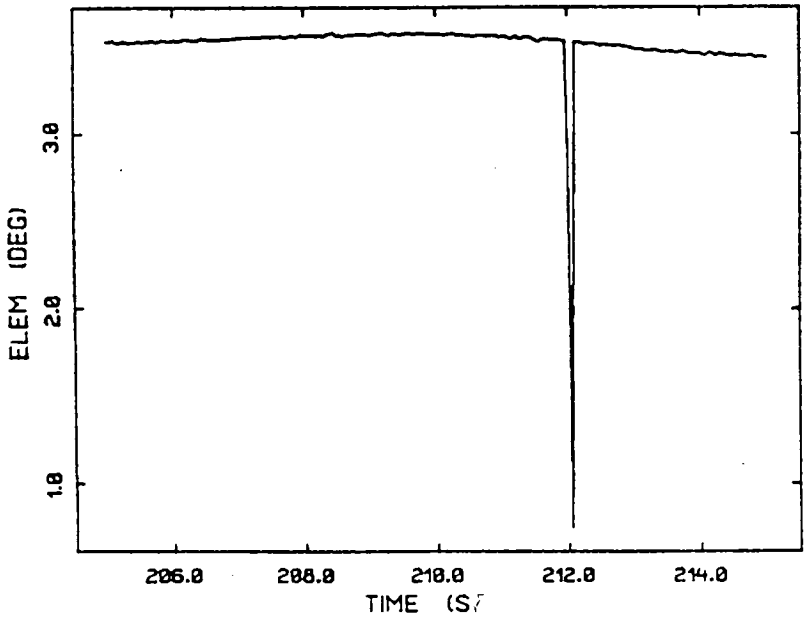

Figure 2.21: MLS elevation dropout at 212 seconds

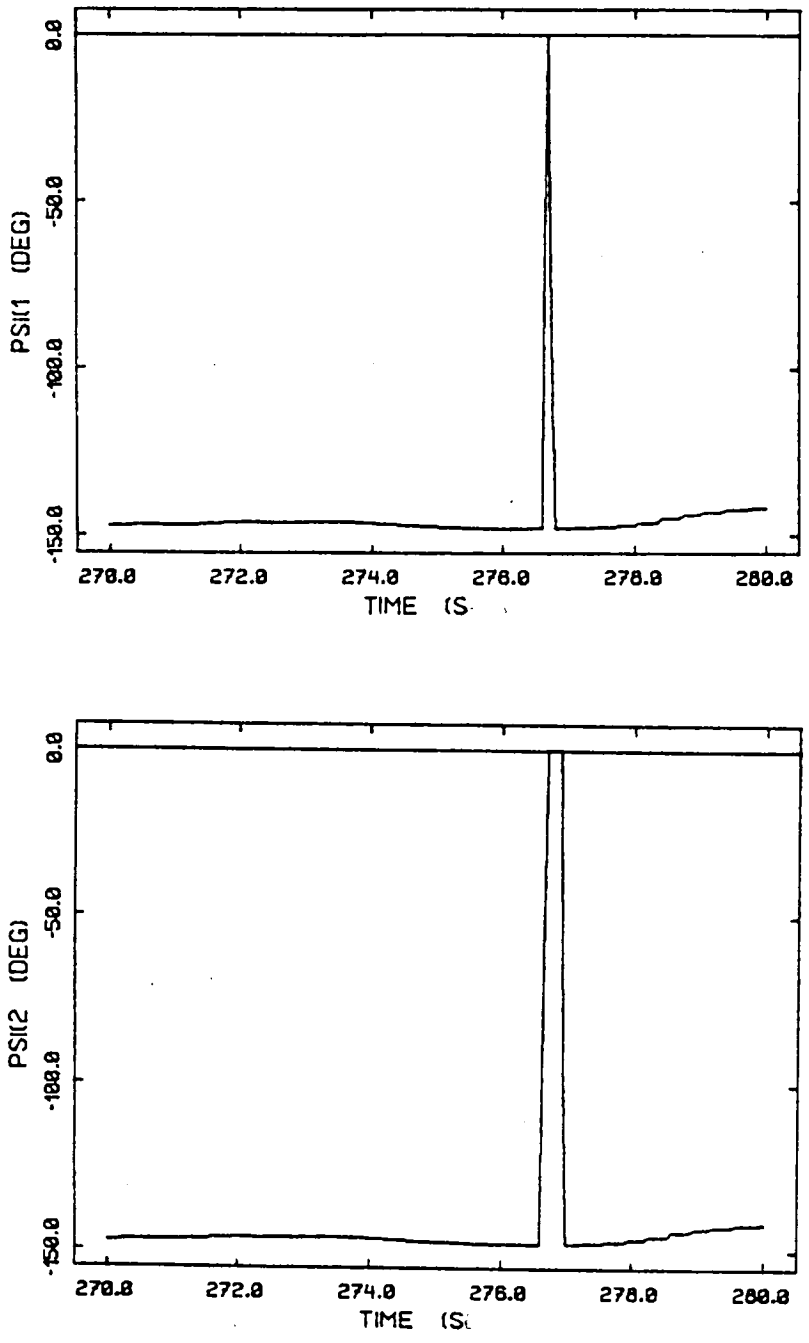

Figure 2.22: IMU yaw channel dropouts at 276.65 seconds

3. PERFORMANCE WITH FLIGHT RECORDED SENSOR DATA

One of the first issues to resolve in the evaluation of FINDS using flight-recorded data is to determine the no-fail filter estimation error performance. In the simulation version of FINDS, this is a simple matter since the true state and bias variables are available from the simulation. Hence, one can directly compute the estimation error by subtracting the estimates from the true variables. On the other hand, in our flight data driven version, the no-fail filter estimation error performance cannot be directly observed since the true states and sensor biases are not available.

Hence, we have investigated various approaches to ascertain, indirectly, the estimation performance of the no-fail filter. For example, one approach is to compute estimates for these true aircraft state, wind and sensor bias variables from sensor measurements using static transformations. In this approach, one can obtain estimates for the aircraft position in the runway frame by transforming the MLS measurements; but these estimates for the true aircraft position coordinates would be poor as compared to the dynamically filtered estimates provided by the no-fail filter. Moreover, there is not enough sensor information to compute aircraft velocity and wind estimates in the same manner.

A second approach is to analyze the values for the estimation error covariance and gains for the no-fail filter. While

gross deviations such as no-fail filter divergence can sometimes be detected in this approach, standard operational performance cannot be determined using this method.

Finally, a third approach is to examine the no-fail filter residuals. If the no-fail filter is operating correctly, i.e. with accurate initial conditions, sensor parameters, etc., then the no-fail filter residual sequence should be approximately a zero mean and white sequence. Any deviation from this behavior would indicate an unsatisfactory performance for the no-fail filter. We have decided to use this approach in our analysis.

The new version of FINDS using flight recorded sensor data will be referred to as "flight data emulation of FINDS" in order to differentiate from the previous simulation version. In the next section, we will describe the developed emulation.

3.1 Emulation Overview

The flight data emulation of FINDS has been obtained first by developing a flight data interface. This was done by replacing the simulation generated measurement set with the flight recorded measurement data. In particular, routines were developed for reading the flight recorded data and assigning them to the appropriate program variables in FINDS.

Secondly, the measurement simulation routines were changed to simulate failures in the flight recorded sensor data. The flight data driven version of FINDS has all of the different

sensor failure injection capability of the previous simulation version. That is, the emulation allows for injecting bias, hardover, increased noise, ramp and scale factor failures into flight recorded sensor measurements.

Concurrent with this development of the flight data interface, major unnecessary blocks simulating the aircraft equations of motion, wind, automatic guidance and control functions, and RSDIMU operation (since the RSDIMU is not in the flight data sensor set) were removed from the emulation since these variables are not needed in a flight data driven version. Since some of the earth related quantities contained in the deleted portions were needed in the estimation/detection algorithms for the compensation of rate gyros for earth's rotation, necessary modifications were made in the software.

In the next two sections we shall describe the major changes made to the FDI algorithm in order to improve performance with flight recorded sensor data.

3.2 Modification to Detectors

Recall from [3] that the FINDS algorithm employs a bank of first order filters called "detectors" driven by the no-fail filter residuals to estimate the levels of postulated sensor failures. That is, the no-fail filter measurement residual sequence and its associated covariance constitute the inputs into the detectors. Hence, the accurate estimation of failure levels

by the detectors, and, consequently, the failure detection performance, depends on the following attributes of the no-fail filter residuals:

- signature of the sensor failure on the residuals
- accuracy of the residual covariance statistics.

As explained by the example in Section 2.7 in [3], the signature of a sensor failure on the no-fail filter residuals determines the identifiability of that failure. In FINDS, the failure signature properties for a specific sensor are, in turn, determined by the sensor noise value used in the design of the no-fail filter, and whether or not the normal operating bias for that sensor is estimated. Hence, if a sensor is not heavily used by the no-fail filter (e.g. if the sensor noise parameter used in the design is large), then the failure signature for that sensor would be less identifiable. Similarly, the accuracy of the no-fail filter residuals covariance, used in the computation of detector gains, determines the failure level estimation, and consequently, failure detection performance of the algorithm.

Clearly, there is a natural conflict between the state estimation and failure detection requirements. That is, if a sensor is noisy, then the no-fail filter would make relatively less use of that sensor output in comparison to other sensors in order to optimize estimation error performance. On the other hand, from a detection point of view, it is desirable to force the no-fail filter to make heavy use of that sensor in order to generate identifiable failure signatures on its residuals.

In our earlier work, sensor noise parameters were chosen by making a compromise between good estimation and detection performance. In our current study, sensor noise parameters are selected in order to optimize the estimation error performance of the no-fail filter. Moreover, the sensor noise parameter values employed in the computation of the no-fail filter measurement residual covariance used by the detectors are now different design variables. In this manner, it has been possible to select values for the second set of sensor noises accurately matching the actual measurement residual covariance of the no-fail filter.

3.3 Decision Rule Change

As discussed in [3], the decision rule in FINDS implements a multiple hypothesis test using a detection window of measurement residuals. Recall that the test is based on the current number of measurement residuals in a detection window of fixed length. That is, for a sampling interval of 0.05 seconds and a detection window of length 0.5 seconds, the test is based on a cyclic repetition of 1,2,3,4,5,6,7,8,9, and 10 measurements. From eqn. (2.53). in [1], the decision rule selects the hypothesis corresponding to the minimum of the likelihood ratios given by

$$\lambda_i(K)=1/2 \sum_{k=1}^{K} r_i'(k)\, R^{-1}(k) r_i(k)-\ln P_i \qquad i=0,1,\ldots,M \tag{3.1}$$

where K is the current number of measurement residuals in the detection window, $r_i(k)$ is the measurement residual at the k'th

instant compensated by the i'th detector, R(k) is the covariance of the no-fail filter measurement residual at the k'th instant, and P_i is the a priori probability of the i'th hypothesis. As discussed in the previous section, in contrast to our earlier simulation work, the covariance R(k) in the decision rule above is different from the computed covariance of the no-fail filter measurement residual sequence.

If the i'th failure mode is the true hypothesis, then each term $r_i^t(k)\ R^{-1}\ r_i(k)$ in the sum in eqn. (3.1) would be a Chi-squared random variable with m degrees of freedom where m is the dimension of the residual vector (i.e. the number of measurements currently used by the no-fail filter). Hence, the sum in eqn. (3.1) would be a Chi-squared random variable with Km degrees of freedom [5]. Normalizing eqn. (3.1) by K/2, our decision logic is equivalent to selecting the hypothesis corresponding to the minimum of:

$$\Delta_i(k) = 1/K \sum_{k=1}^{K} r_i^t(k)\ R^{-1}(k)\ r_i(k) - 2/K\ \ln P_i \qquad (3.2)$$
$$i=0,1,\ldots,M$$

Examination of eqn. (3.2) above shows that the average sum of squares of the residuals is effectively compared with a monotonically decreasing threshold.

Hence, the effect of a priori probabilities diminish towards the end of a detection window. An analysis of false alarms with flight recorded data revealed that most of the false alarms were near the end of the detection window due to the decision rule's

attribute described above. Therefore, we have changed the decision rule to choose the hypothesis corresponding to the minimum of:

$$L_i(K)=1/K \sum_{k=1}^{K} r_i^{!}(k)\ R^{-1}(k)\ r_i(k) + d_i \qquad i=0,1,\ldots,M \tag{3.3}$$

where the thresholds d_i are now chosen from Chi square tables for a given false alarm rate specification.

3.4 Emulation Description

In this section, we describe the characteristics of the flight recorded data used in our present study. In particular, we present a description of the nominal flight path of the aircraft, and important aircraft state variable time histories as estimated by the no-fail filter in FINDS.

The flight recorded sensor data covers 298 seconds of flight, at a sampling frequency of 20Hz for each sensor. Thus, a sampling interval of 0.05 seconds is used in the emulation runs -- which is the same update rate used in all previously reported simulation runs. Also, the recorded sensor data begins with the aircraft already within MLS coverage boundaries; so that all the FINDS algorithm (no-fail filter, detectors, decision logic) is initiated at the start of the emulation run.

Figures 3.1-3 show the aircraft state estimate time histories for the nominal emulation run, provided by the no-fail filter using the appropriate sensor noise parameters. In

contrast to earlier simulation studies, MLS sensor noise has been assumed to be white based on the sensor error analysis in the last chapter.

The A/C ground track, altitude profile, and horizontal runway coordinate time histories are depicted in Figure 3.1-3. These figures show the sequencing of the various flight segments as the A/C performs its approach to runway, altitude hold, alignment with runway, and finally "touch-and-go" maneuvers. Initially, the x and y position coordinates in the runway frame are approximately (-17000 m, -4800 m), and the initial ground track is oriented roughly 30° relative to the runway. A bank maneuver at constant altitude is executed (from 100 -140

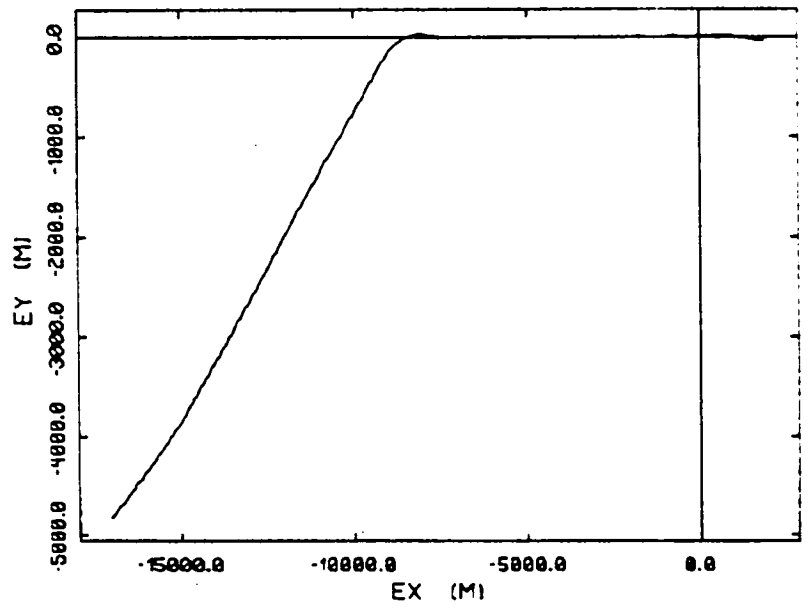

Figure 3.1: Estimated aircraft ground track

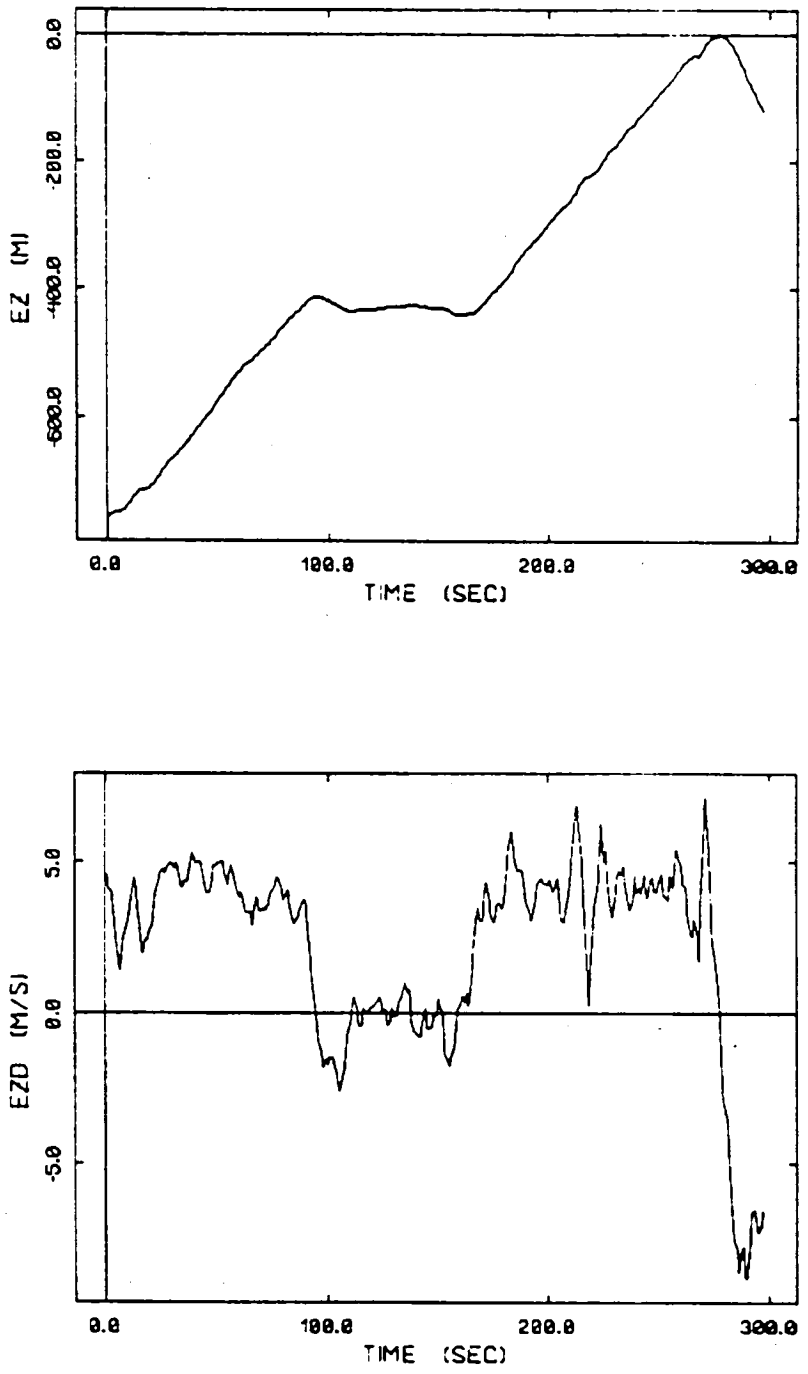

Figure 3.2: Estimated altitude and vertical velocity profiles

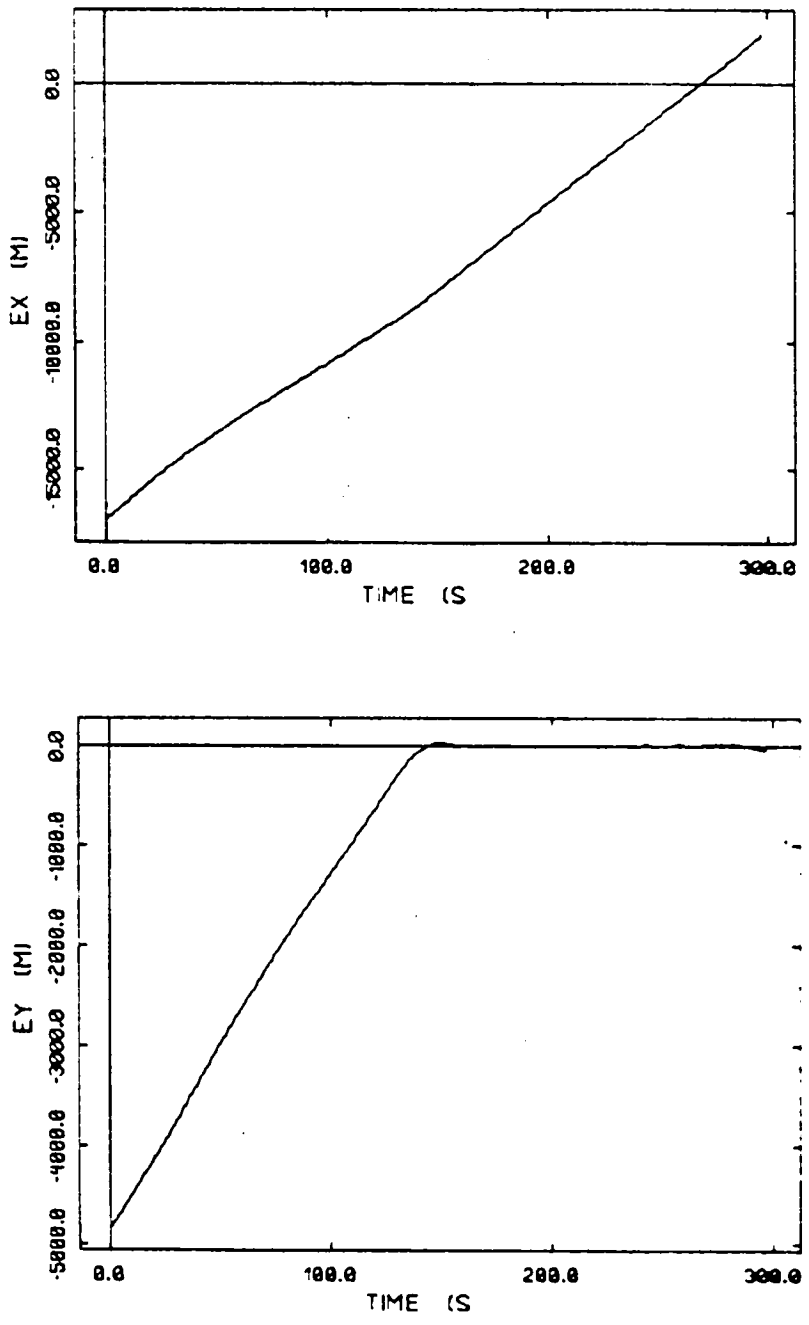

Figure 3.3: Horizontal runway position time histories

seconds) which brings the flight track in alignment with the runway. At the end of this maneuver (144 seconds), the A/C is exactly aligned with the runway (i.e. x and y coordinates of (-8400 m, 0 m)). This flight segment lasts till touchdown (277 seconds). In this flight segment, radar altimeter measurements are turned on at approximately 266 seconds replacing the MLS elevation sensors. The final portion of the flight segment between 277- 298 seconds depicts the A/C in a take-off and slow bank maneuver, finally ending at position coordinates (1940 m, -46 m).

The altitude profile curve shows the A/C initially at a height of 760 meters with a nearly constant sink rate of approximately 4 m/s until touchdown. Also note that the A/C altitude stays almost constant during the runway alignment maneuver described above. After touchdown, we see a higher climb rate of approximately 7-8 m/s in the final segment of the flight path. The final altitude of the A/C at 298 seconds is 125 meters.

The A/C flight path and altitude profile can be summarized by the following mapping, which will be convenient for later reference.

1)	Descent:	A/C is descending at constant sink rate in a flight path oblique to the runway (0-100 seconds).
2)	Alignment maneuver:	A/C is maneuvering to align with the runway at constant altitude (100-140 seconds).
3)	Landing maneuver:	A/C is parallel to runway and descending for touchdown (140-277 seconds).

4) Take-off: A/C is executing a bank maneuver and climbing (277-298 seconds).

Figure 3.4 displays the no-fail filter estimates for the aircraft horizontal velocity components in the runway frame. These figures show that the aircraft velocity has components both in the x and y runway axes up to 150 seconds. After the alignment maneuver with the runway, the aircraft velocity is mostly along the x axis, except for small variations due to maneuvers in order to stay aligned with the runway. The vertical velocity component estimate time history depicted in Figure 3.2 is in agreement with the aircraft altitude profile estimate shown in the same figure.

The no-fail filter attitude estimates for the emulation run are shown in Figures 3.5-6. As can be seen from the roll attitude estimate time history in Figure 3.5, significant aircraft bank maneuvers occur during the flight segments from 20-30, 130-160, 260-275 seconds. Pitch attitude estimate time histories show that the aircraft is pitching down at an angle of 2^{o}-4^{o} during most of the emulation run, except for the flight segments where the altitude hold and final take-off maneuvers are executed. Yaw attitude estimate time history shown in Figure 3.6 reflects the low frequency content in this variable in contrast to roll and pitch attitudes.

Figure 3.4 shows the no-fail filter estimates for the horizontal winds in the runway frame. The estimates indicate essentially a constant crosswind of about 10 m/s throughout the emulation run.

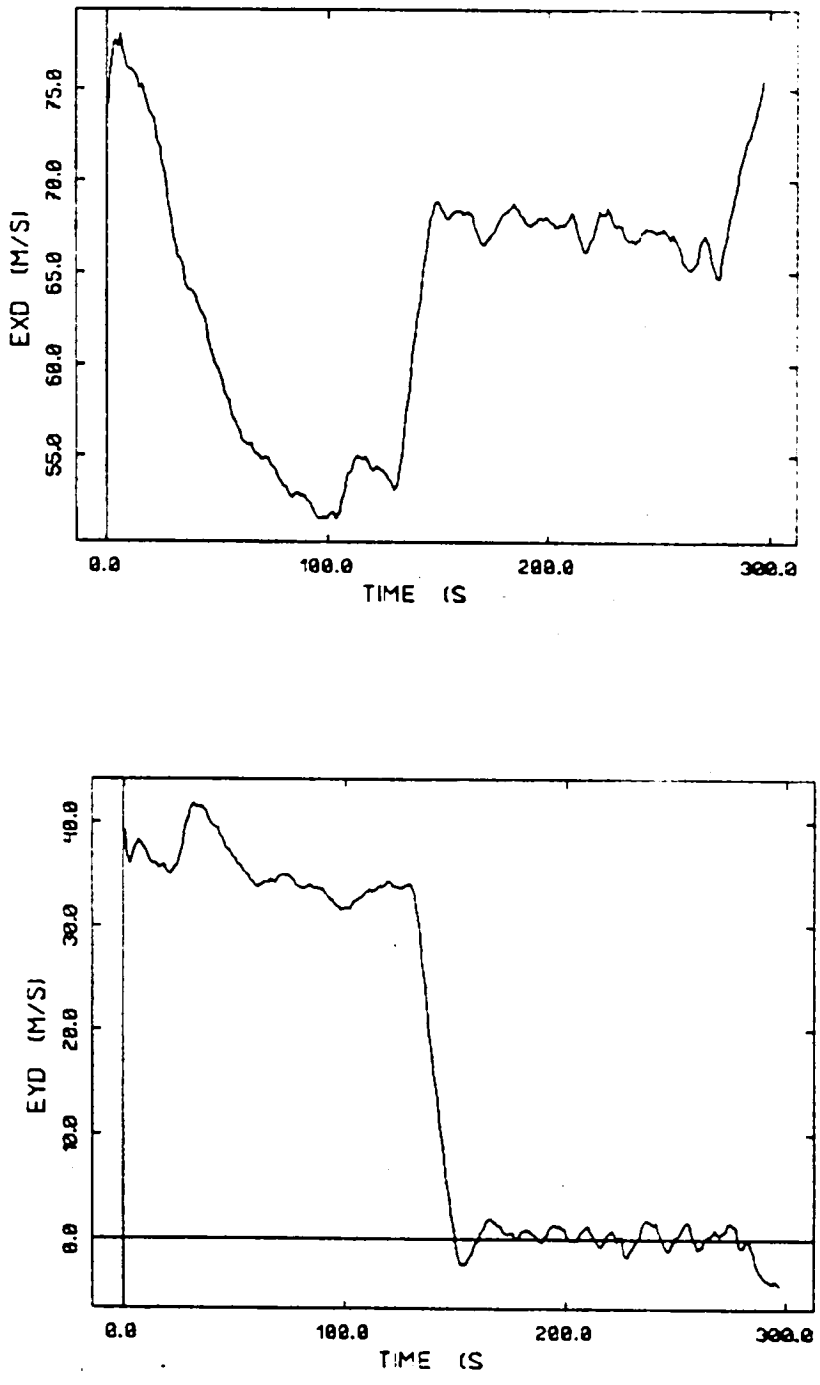

Figure 3.4: Horizontal velocity estimate time histories

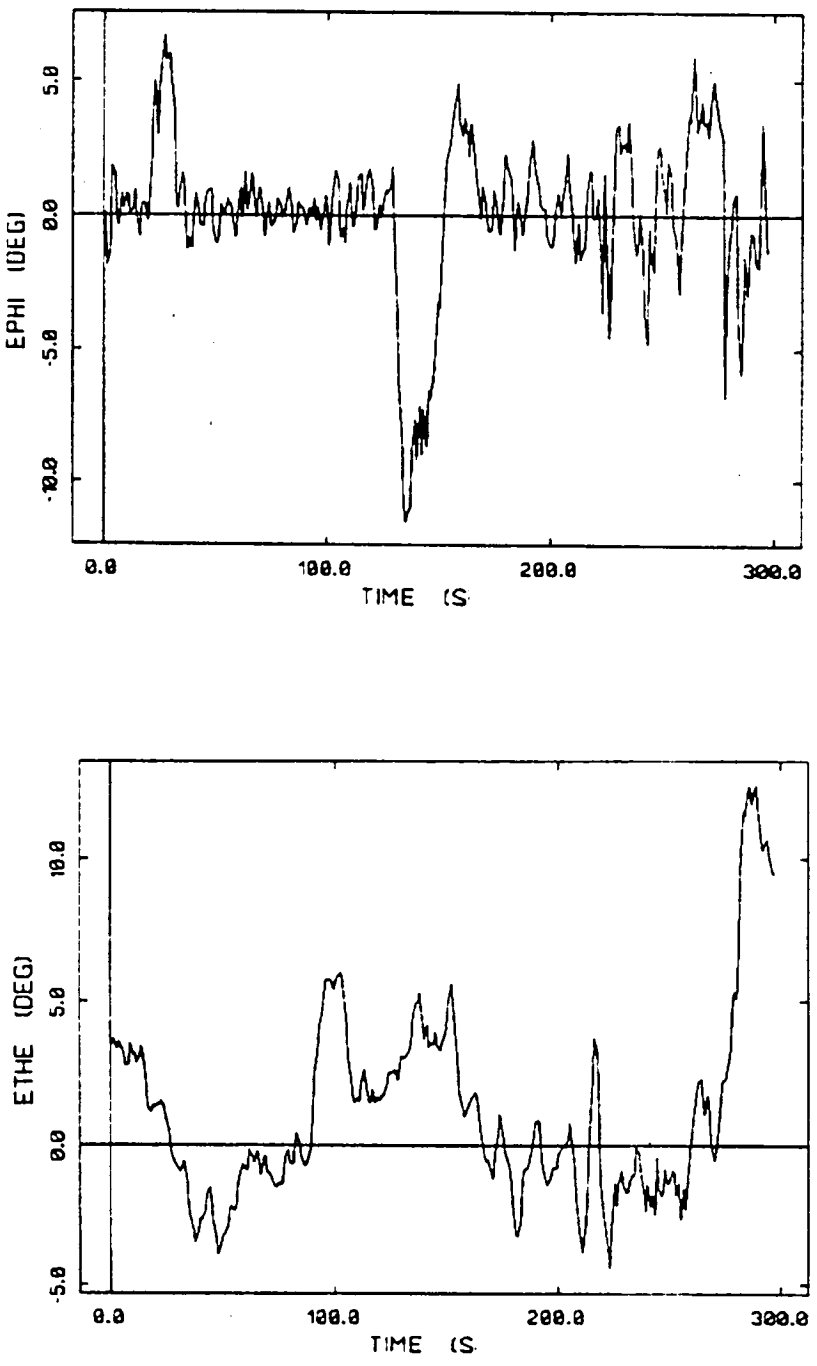

Figure 3.5: Roll and pitch attitude estimates

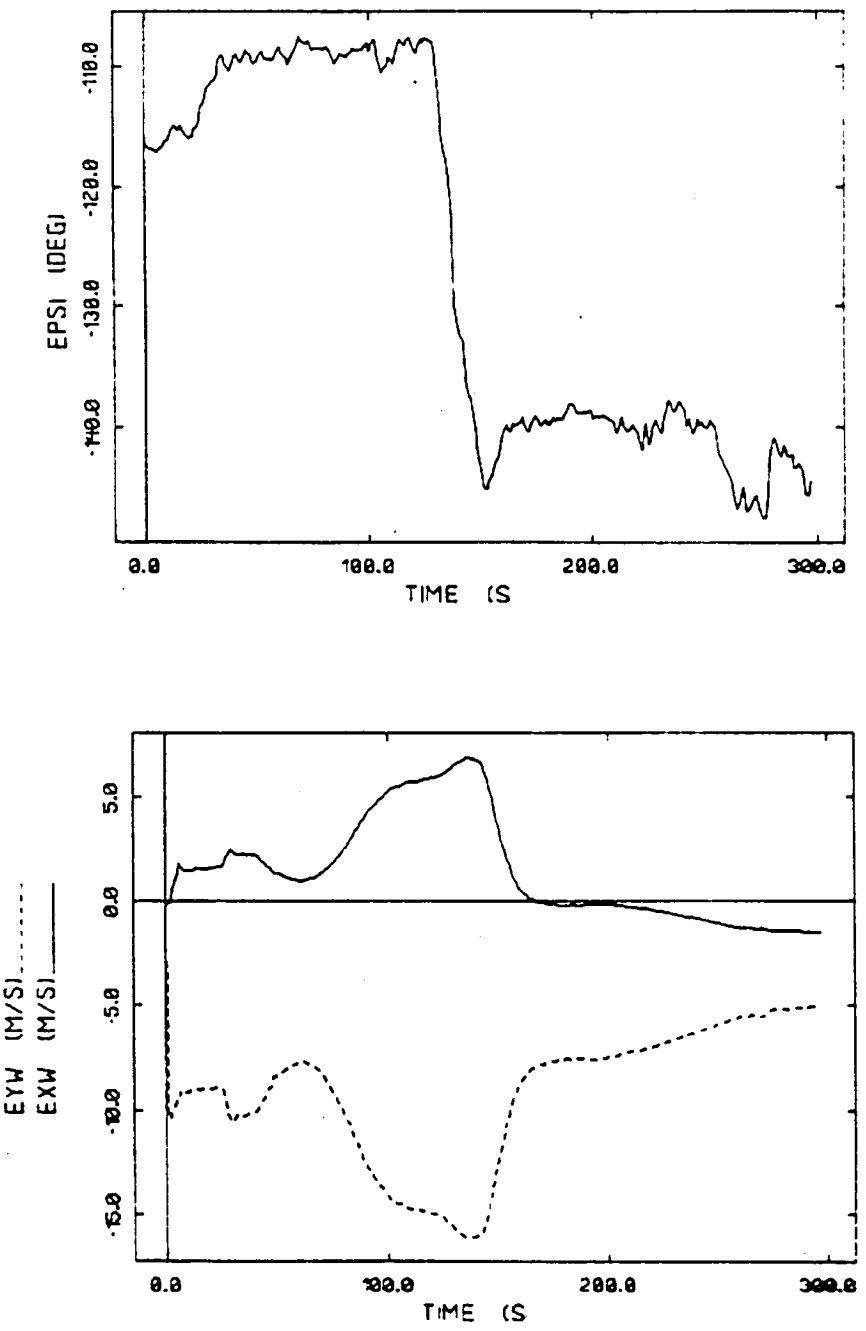

Figure 3.6: Yaw attitude and horizontal wind estimates

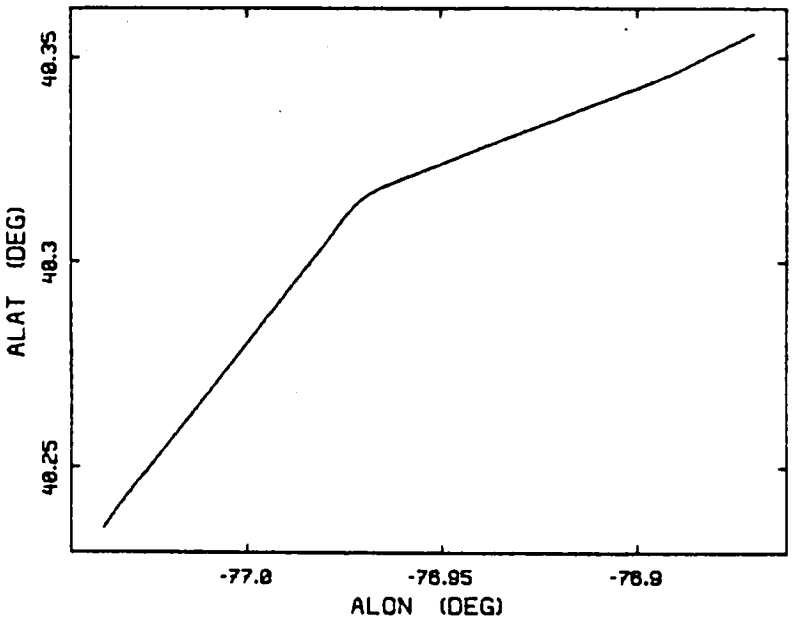

Figure 3.7: Aircraft latitude vs. longitude track

The aircraft latitude and longitude estimates are depicted in Figure 3.7. As expected, there is no significant change in those variables from the initial conditions.

Before proceeding on to the performance evaluation of FINDS, we make a few concluding comments about the A/C profiles above. First, referring back to Section 2.4 on data dropouts, the MLS and IMU yaw measurement dropouts around 276-277 seconds can be attributed to the proximity to MLS antennas during the A/C

"touch-and-go" maneuver. In contrast, the MLS measurement dropouts at 212 seconds appear to be genuine sensor or recording failures. The sensor characteristics are generally in agreement with the previously reported simulation results for FINDS.

3.5 Performance With No Failures

The first step in evaluating the flight data driven version of FINDS is to determine the estimation error performance of the no-fail filter in the FINDS algorithm. The performance of the no-fail filter is important since this performance ultimately affects the failure detection and isolation attributes of the algorithm. In section 3.2 above, we have discussed the changes made to the FINDS algorithm in order to minimize the conflict between the estimation and detection functions.

As stated in the beginning of this chapter, due to the unavailability of the true A/C states and sensor biases in our emulation, we analyze the no-fail filter performance by examining the filter residual sequences. The specific sensor noise parameters used in the design of the no-fail filter are obtained, from the statistical analysis performed on the replicated sensor difference signals (see Chapter 2, Tables 2.1-2). In this section, two specific baseline emulation run results are presented; one without the detectors implementing the failure detection and isolation (FDI) algorithm, and the other with the detectors on but with no injected failures.

First, we have decided to estimate the normal operating biases only for the input sensors, i.e. the body mounted linear accelerometers (a_x, a_y, a_z) and the rate gyros (p, q, r). From the flight data analysis, we see that these sensors have a higher bias to noise standard deviation ratio compared to other sensors such as MLS, IMU, and IAS. The other rationale for this choice is to keep the size of the bias-estimator filter block down to an acceptable size. Figures 3.8-10 show the bias estimate time histories as obtained from the baseline run with the detectors off. As seen from these figures, it takes approximately 60-70 seconds for the no-fail filter to reach the steady state bias estimate in the case of the linear accelerometers. Of the three sensors, the longitudinal accelerometer shows the highest fixed bias level of approximately -0.19 m/s^2. The steady-state bias estimate for the lateral accelerometer is roughly 0.075 m/s^2.

The convergence rate of the rate gyro bias estimates to their steady-state levels is faster than that for accelerometer bias estimates as seen from Figures 3.9-10. The bias-estimator filter, in this case, needs only 20-30 seconds to converge to the steady state bias levels which are -0.27 deg/s for the roll rate (p), -0.23 deg/s for the pitch rate (q) and 0.14 deg/s for the yaw rate (r). The reason for the rapid convergence of rate gyro bias estimates, relative to that for accelerometer bias estimates, is the availability of closely coupled sensors such as IMU measurements.

Variable	Init. Est.	Uncertainty (S.D.)	Units
States:			
x-rw	-1.4403E+04	4.0000E+01	m
y-rw	-4.2300E+03	4.0000E+01	m
z-rw	-7.3396E+02	3.0000E+01	m
x-dot-rw	7.6505E+01	4.0000E+00	m/s
y-dot-rw	3.7186E+01	4.0000E+00	m/s
z-dot-rw	3.9929E+00	1.2500E+00	m/s
phi (roll)	3.5800E+00	5.0000E-01	deg
theta (pitch)	2.5800E+00	5.0000E-01	deg
psi (yaw)	3.1760E+01	1.5000E+00	deg
x-wind-rw	0.0000E+00	7.5000E-01	m/s
y-wind-rw	-1.0302E+01	7.5000E-01	m/s
Biases:			
longit. accel.	0.0000E+00	3.0480E-01	m/s/s
lateral accel.	0.0000E+00	3.0480E-01	m/s/s
vertical accel.	0.0000E+00	3.0480E-01	m/s/s
roll rate gyro	0.0000E+00	2.5600E-01	deg/s
pitch rate gyro	0.0000E+00	2.5600E-01	deg/s
yaw rate gyro	0.0000E+00	2.5600E-01	deg/s

NOTE: All states with subscript -rw are with reference to the runway coordinate frame.

Table 3.1: No-fail filter initial estimates

Variable	Noise S.D. Per Repl.	Replications Used	Units
Process Noises:			
longit. accel.	5.0000E-02	1	m/s/s
lateral accel.	7.0000E-02	1	m/s/s
vertical accel.	1.0000E-02	1	m/s/s
roll rate gyro	5.0000E-02	1	deg/s
pitch rate gyro	5.0000E-02	1	deg/s
yaw rate gyro	5.0000E-02	1	deg/s
x-wind-rw	0.0000E+00	N/A	m/s
y-wind-rw	0.0000E+00	N/A	m/s
Measurement Noises:			
MLS azimuth	6.0000E-02	2	deg
MLS elevation	6.0000E-02	2	deg
MLS range	8.5000E+00	2	m
IAS	1.5000E+00	2	m/s
IMU roll	2.5000E-01	2	deg
IMU pitch	5.0000E-01	2	deg
IMU yaw	3.0000E-01	2	deg
Radar altimeter	1.0000E+00	0	m

Table 3.2: Design values for no-fail filter noise parameters

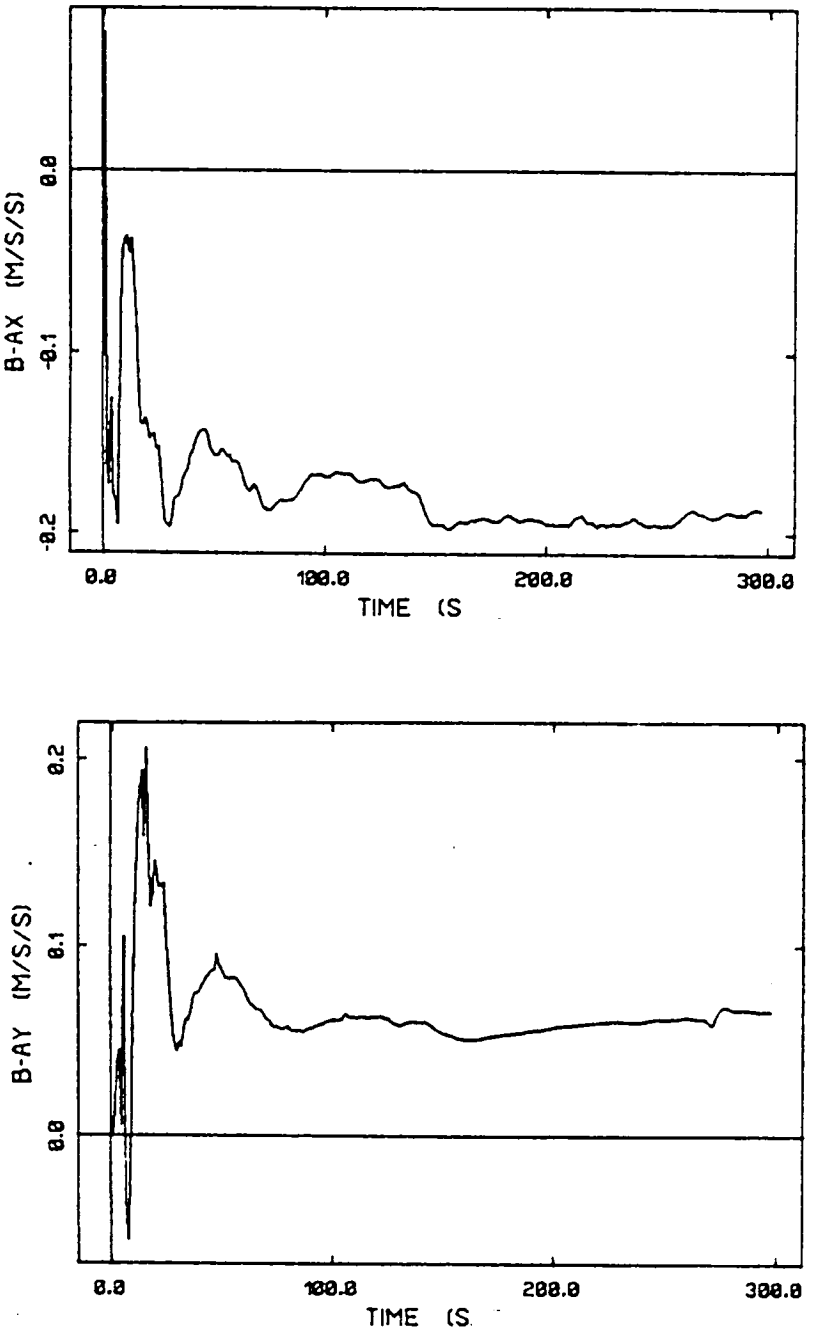

Figure 3.8: Longitudinal and lateral accelerometer bias estimates

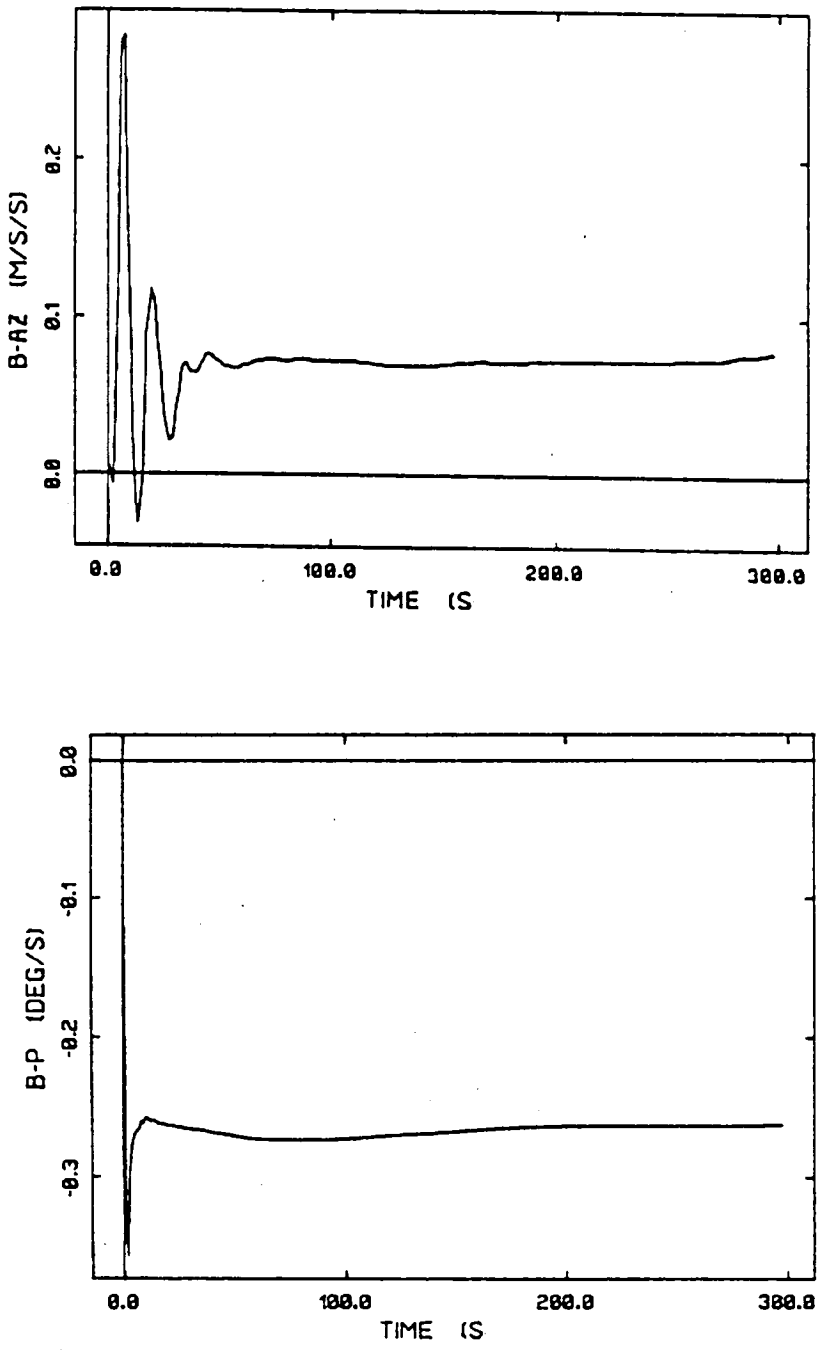

Figure 3.9: Vertical accelerometer and roll rate gyro bias estimates

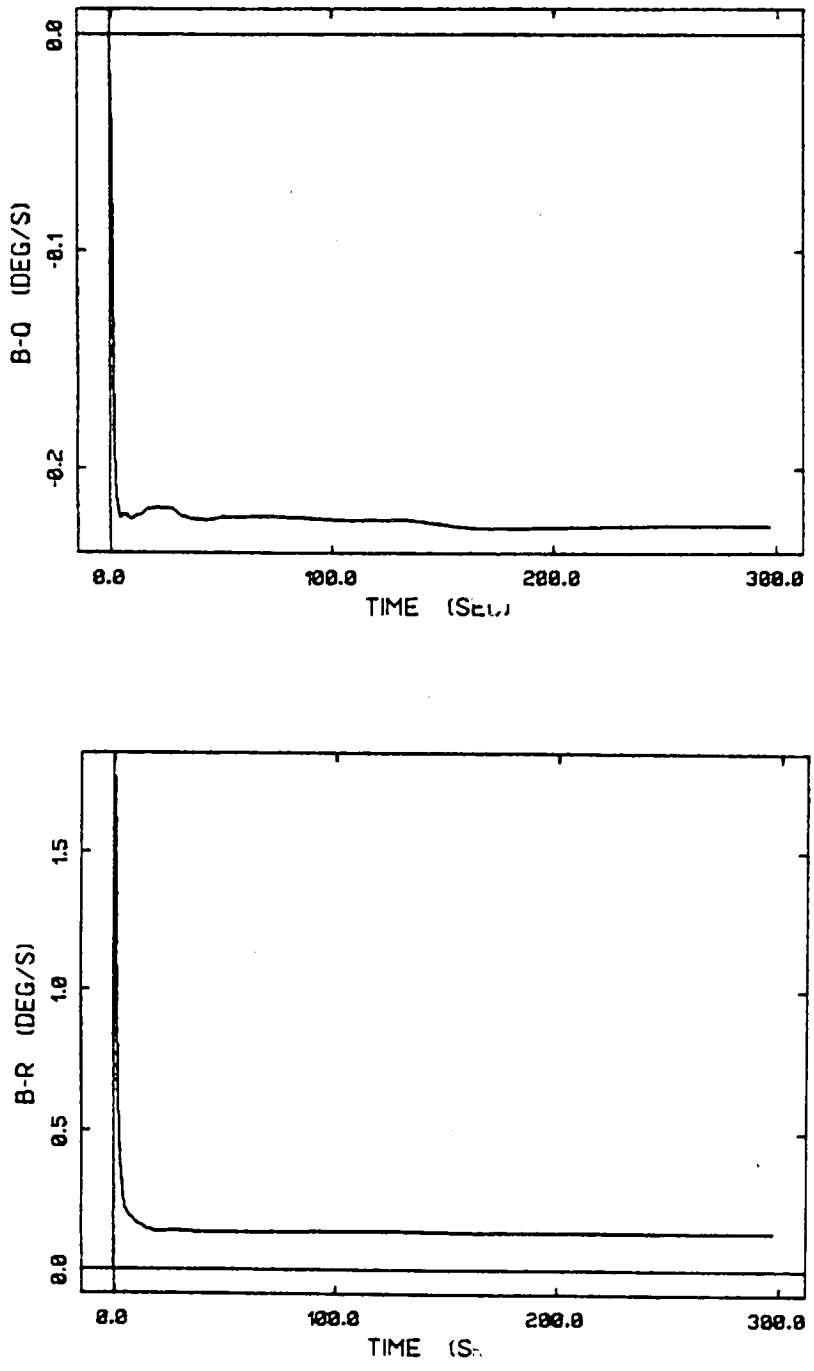

Figure 3.10: Pitch and yaw rate gyro bias estimates

The no-fail filter initial conditions for the state and normal operating bias estimates along with the standard deviation of the initial uncertainty for these variables are shown in Table 3.1. The process and measurement noise statistics used in the design of the no-fail filter are given in Table 3.2. These parameter values are largely based on the flight data analysis presented in Chapter 2. Note that the noise parameter design values are given in a per replication manner -- to reflect the fact that the actual measurement noise statistics used depend on the number of replications of a given sensor. Also, the wind process noise is replication independent as it does not relate to a physical sensor.

The no-fail filter measurement residual time histories are shown in Figures 3.11-14 for the same emulation run. As expected, these measurement residual sequences show the dependence of estimation error on aircraft maneuvers during which the linearity assumptions employed in the no-fail filter are most seriously violated. For instance, the MLS azimuth and range, IAS, and the IMU roll and yaw attitude measurement residuals depicted respectively in Figures 3.11-14, exemplify such a case. Note also that the MLS elevation and radar altimeter measurements residual sequences given in Figures 3.11 and 3.14 have time scales corresponding to segments of the flight data during which these instruments are active.

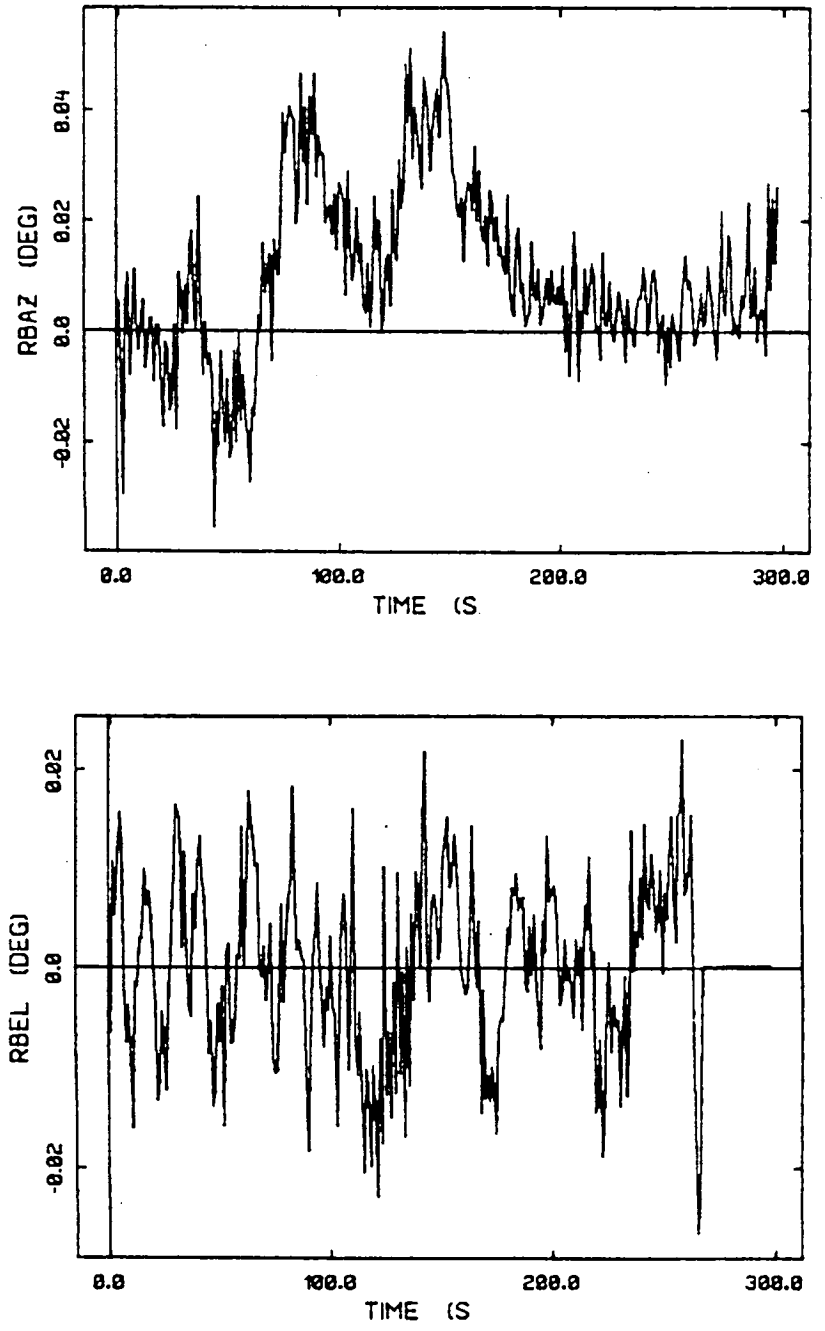

Figure 3.11: No-fail filter residuals for MLS azimuth and elevation

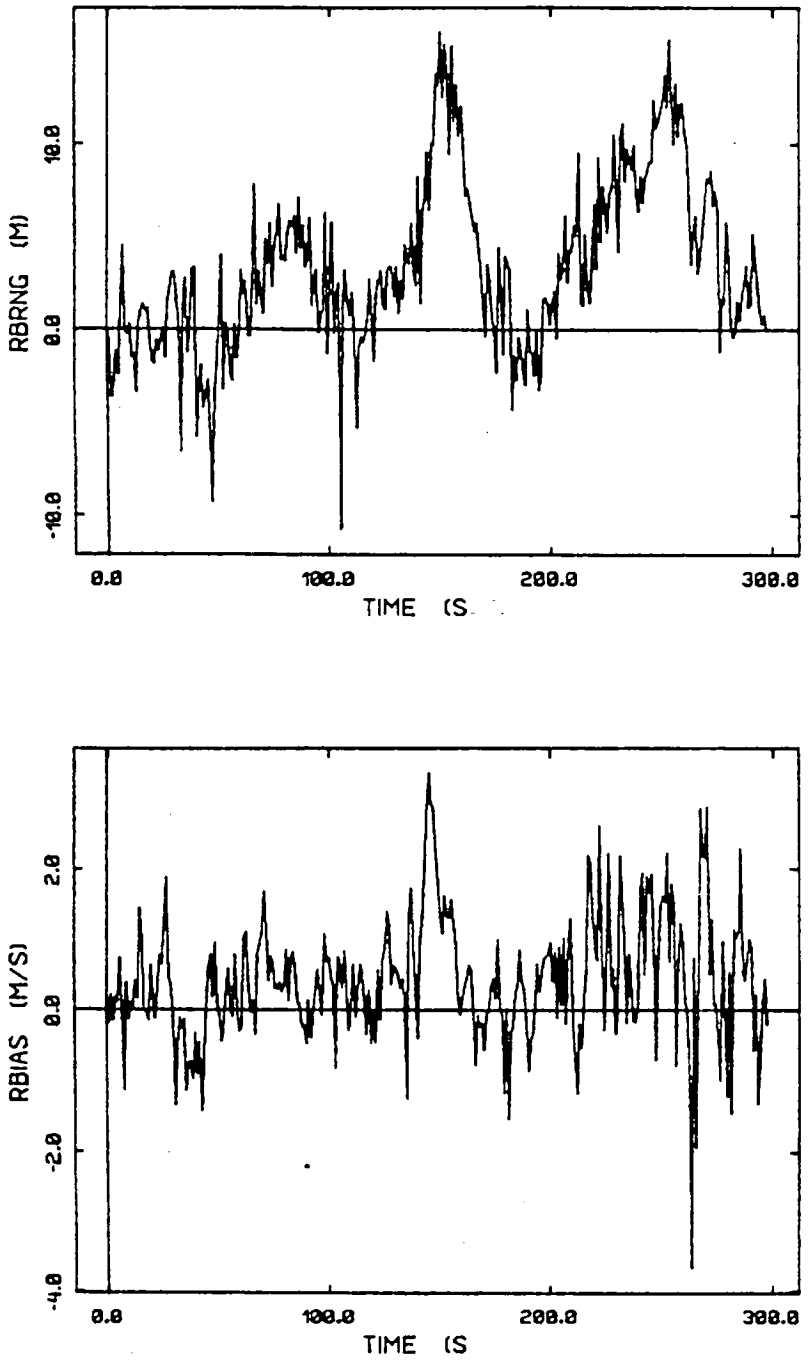

Figure 3.12: No-fail filter residuals for MLS range and IAS

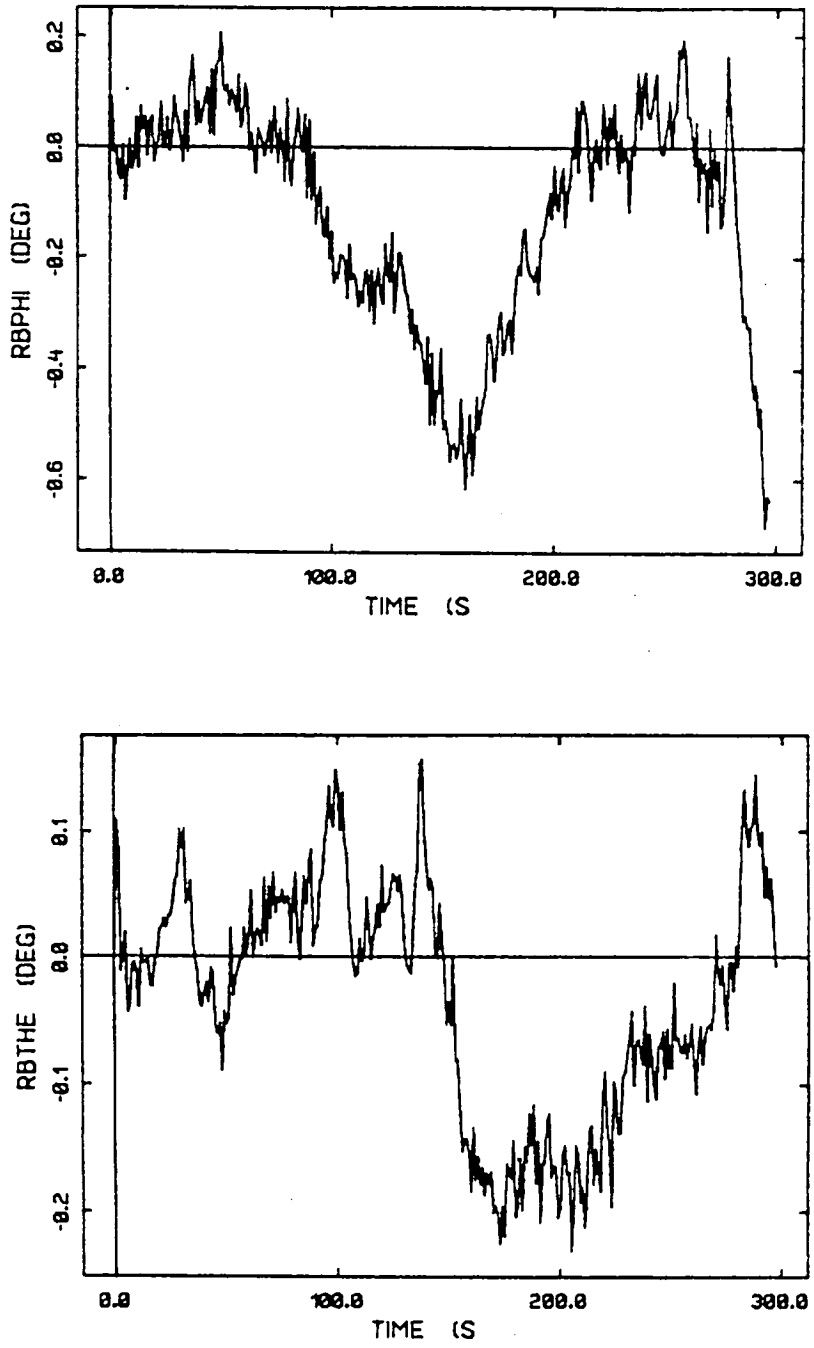

Figure 3.13: No-fail filter residuals for IMU roll and pitch

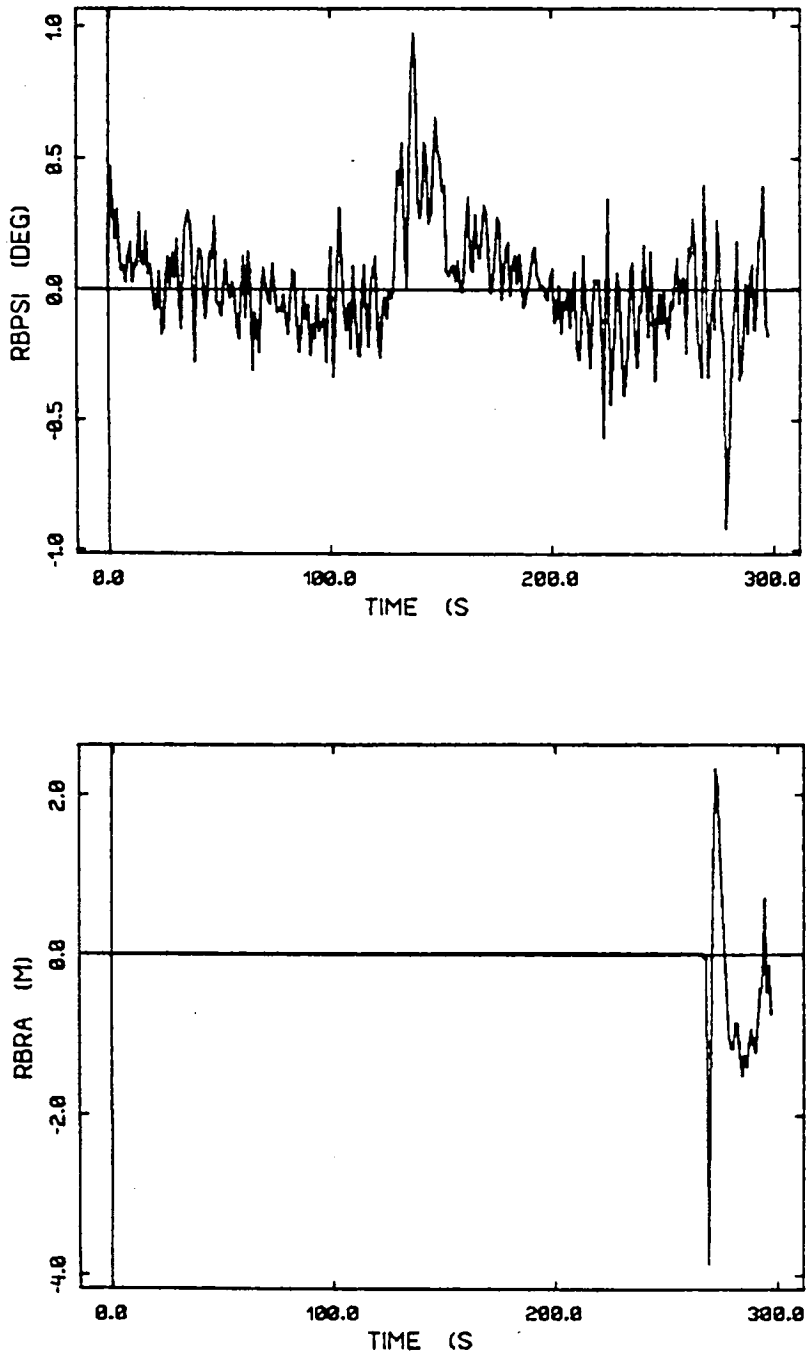

Figure 3.14: No-fail filter residuals for IMU yaw and radar altimeter

Sensor Type	Computed Statistics Sample Mean	Std. Dev.	Units
MLS Azimuth	0.0106	0.0153	deg
MLS Elevation	0.00015	0.0093	deg
MLS Range	3.4089	4.5081	m
IAS	0.3995	0.9295	m/s
IMU Roll	-0.1187	0.2024	deg
IMU Pitch	-0.0324	0.0938	deg
IMU Yaw	0.0154	0.2218	deg
Radar Altimeter	-0.4589	1.0983	m

NOTE: -- MLS Elevation residuals used from T=0 seconds to T=266 seconds.

-- Radar Altimeter residuals used from T=267 seconds to T=298 seconds.

Table 3.3: Computed statistics for no-fail filter residual sequences (baseline run -- detectors off)

Table 3.3 contains the computed sample means and standard deviations for the no fail filter residual sequences over the entire emulation run. Note that the radar altimeter and MLS elevation residual statistics were obtained by using the residual values only in the region where these sensors are active i.e. MLS elevation during 0-266 seconds, and the radar altimeter during 267-298 seconds. These empirical statistics can be used to

investigate the no fail filter performance by comparing them to the sensor measurements difference signal statistics (Table 2.1, Chapter 2). From eqn. (2.37) in [1], we have the following functional model for the no-fail filter measurements:

$$y^i(k) = h(x(k)) + b_y^i + v^i(k) \quad i=1,2 \tag{3.4}$$

where y^i is the i'th replication of the measurement vector at time k, x(k) is the aircraft state vector at the k'th instant, h is the nonlinear transformation mapping the state into the measurements, b_y^i is the measurement bias vector for the i'th replication, and $v^i(k)$ is the zero mean, white measurement noise for the i'th replication. Since the no-fail filter uses the average of the replicated measurements, the no-fail filter measurement residual sequence will be given by:

$$r(k+1) = h(x(k+1)) - h(\hat{x}(k+1/k)) + \bar{b}_y + \bar{v}(k) \tag{3.5}$$

where $\bar{b}_y = (b^1+b^2)/2$ and $\bar{v}(k)=(v^1(k) + v^2(k))/2$. This expression follows since, in the present emulation, none of the measurement biases are estimated. Expanding h(x(k+1)) at $\hat{x}(k+1/k)$, we get

$$r(k+1) \simeq H(\hat{x}(k+1/k))\, \tilde{x}(k+1/k) + \bar{b}_y + \bar{v}(k) \tag{3.6}$$

where $H(\hat{x}(k+1/k))$ is the measurement partial matrix defined by eqn. (2.19) in [1] and $\tilde{x}(k+1)$ is the state estimation error defined by $\tilde{x}(k+1) = x(k+1) - \hat{x}(k+1/k)$. Examination of eqn. (3.6) above suggests that the sample mean and standard deviations of

the no-fail filter residual sequences would have a good indication of its estimation error performance.

From the statistical analysis of replicated sensor channel differences, the standard deviation of the average noise in $\bar{v}(k)$ can be computed. Unfortunately, this analysis does not yield the average bias but the difference of biases in the replicated versions. As an approximation, we have compared the rms values of the difference signals to the rms values of the measurement residuals. These comparisons indicate, in general, a good estimation error performance for the no-fail filter. For instance, for the IAS sensor, rms value increased from 0.94 m/s to 1.01 m/s indicating an rms error of 0.07 m/s. Similarly, for the IMU roll attitude sensor, the increase in the rms error is 0.1 degrees.

The second baseline run is made with the detectors on, without any injected failures, and using the same sensor noise parameters. As discussed in Section 3.2, the advantage in differentiating the sensor noise parameters used in the no-fail filter from those used in the detectors is to keep the estimation performance at its nominal best while fine tuning the failure detection and isolation performance and sensitivity. Thus, in the second baseline run, the no-fail filter estimation performance is exactly the same as in the first baseline case.

The fault tolerant system detector parameters are summarized in Tables 3.4 and 3.5. Table 3.4 gives the test threshold for

each sensor, detector estimation window length, standard deviations of the estimation information used for detector resetting and the sensor noise parameters used by the detection logic. Table 3.5 shows the bias and failure threshold levels used in the healer module. The healer window length used is 3 seconds in all runs.

During the preliminary second baseline run, a false-alarm in yaw rate gyro at around 136 seconds into the emulation was encountered with healing within 3 seconds. This was later traced back to the noisy measurement yaw attitude data in the 130-140 seconds time span. Hence, the yaw attitude sensor noise standard deviation was increased from a value of 0.3° to 0.4°, reflecting the inaccuracy in this sensor. The sample time-line file for the second baseline emulation run is shown in Table 3.6. Referring to this table, MLS and FINDS filter and detectors are turned on at 0.05 seconds. Without encountering any false alarms, the radar altimeter is turned on around 266.2 seconds at an altitude of 30 meters. This is accomplished by collapsing the MLS-elevation measurements. Finally, the run ends at 298.05 seconds (the end of flight recorded data).

At this stage, the estimation performance of the no-fail filter, and the false alarm performance of the detectors are now optimized. In the next section, we discuss the failure detection performance with flight recorded sensor data.

Detectors assume M.L.S. noise is WHITE
Detector Window Length = 0.500 seconds

Sensor Type	Test Threshold	Estim. Window (s)	Estim. Info. (S.D.)	Noise S.D. (SIGD)	Units
Singular Failures:					
longit. accel.	2.0018E+01	3.00	9.29E-03	5.00E-02	m/s/s
lateral accel.	2.0018E+01	3.00	9.29E-03	7.00E-02	m/s/s
vertical accel.	2.0018E+01	3.00	9.29E-03	1.00E-01	m/s/s
roll rate gyro	2.0018E+01	3.00	0.00E+00	5.00E-02	deg/s
pitch rate gyro	2.0018E+01	3.00	0.00E+00	5.00E-02	deg/s
yaw rate gyro	2.0018E+01	3.00	0.00E+00	5.00E-02	deg/s
MLS azimuth	2.0018E+01	.50	0.00E+00	3.00E-02	deg
MLS elevation	2.0018E+01	.50	0.00E+00	2.00E-02	deg
MLS range	2.0018E+01	.50	0.00E+00	8.00E+00	m
IAS	2.0018E+01	.50	0.00E+00	1.50E+00	m/s
IMU roll	2.0018E+01	.50	0.00E+00	2.50E-01	deg
IMU pitch	2.0018E+01	.50	0.00E+00	2.00E-01	deg
IMU yaw	2.0018E+01	.50	0.00E+00	4.00E-01	deg
Radar altimeter	2.0018E+01	.50	0.00E+00	1.00E+00	m
Simultaneous Multiple Failures:					
MLS azimuth	4.9246E+01				
MLS elevation	4.9246E+01				
MLS range	4.9246E+01				

Table 3.4: Detector parameters

3.6 Performance with Injected Bias Failures

In this section, we present the results for emulation runs where various bias failures are injected into the sensor flight data, and discuss the failure detection and isolation performance of the FINDS algorithm. The reason for the selection of bias failures in this analysis follows from our earlier simulation

Healer Window Length = 3.000 seconds

Sensor Type	Bias Est Threshold	Failure Est Threshold	Decision Threshold (Square Units)	Units
longit. accel.	3.000E-01	5.000E-01	-2.8317E+00	m/s/s
lateral accel.	3.000E-01	5.000E-01	-5.5501E+00	m/s/s
vertical accel.	3.000E-01	5.000E-01	-1.1327E-01	m/s/s
roll rate gyro	2.000E-01	5.000E-01	-2.9444E-02	deg/s
pitch rate gyro	2.000E-01	5.000E-01	-2.9444E-02	deg/s
yaw rate gyro	2.000E-01	5.000E-01	-2.9444E-02	deg/s
MLS azimuth	9.000E-02	1.000E-01	-8.4800E-02	deg
MLS elevation	9.000E-02	1.000E-01	-8.4800E-02	deg
MLS range	9.000E+00	3.000E+01	-1.7019E+03	m
IAS	1.700E+00	3.000E+00	-3.7698E+00	m/s
IMU roll	3.000E-01	5.000E-01	-3.6805E-01	deg
IMU pitch	3.000E-01	5.000E-01	-1.4722E+00	deg
IMU yaw	3.000E-01	5.000E-01	-5.3000E-01	deg
Radar altimeter	6.000E-01	1.000E+00	-5.8889E+00	m

Table 3.5: Sensor healer parameters

```
TIME = 0.05 s.          EVENT : MLS Coverage Begins / Filter Turn On

N-F FILTER STATES :
-1.4403E+04 -4.2300E+03 -7.3396E+02  7.6505E+01  3.7186E+01  3.9929E+00
 3.5800E+00  2.5800E+00  3.1760E+01  0.0000E+00 -1.0302E+01
BIAS FILTER ESTIMATES :
 0.0000E+00  0.0000E+00  0.0000E+00  0.0000E+00  0.0000E+00  0.0000E+00


TIME = 266.20 s.        EVENT : Radar Altimeter Turn On

N-F FILTER STATES :
-2.5095E+02  3.7080E+00 -3.0443E+01  6.5319E+01  2.9840E-01  3.1622E+00
 2.7572E+00  1.1144E+00 -3.5847E+02 -1.3581E+00 -5.5324E+00
BIAS FILTER ESTIMATES :
-1.8671E-01  6.0690E-02  7.3919E-02 -2.6363E-01 -2.2717E-01  1.3536E-01


TIME = 298.05 s.        EVENT : End of Emulation Run

N-F FILTER STATES :
 1.9400E+03 -4.5618E+01 -1.2560E+02  7.5962E+01 -4.6090E+00 -6.8641E+00
 2.4479E-01  9.5560E+00 -3.5698E+02 -1.5168E+00 -5.0799E+00
BIAS FILTER ESTIMATES :
-1.8634E-01  6.4670E-02  1.4110E-01 -2.6305E-01 -2.2730E-01  1.3561E-01
```

==========

NOTE THAT IN ALL THE TIME-LINE FILES, THE N-F FILTER STATES AND BIAS FILTER STATES ARE ORDERED (ALONG WITH THEIR UNITS) AS PER TABLE 3.1 (page 56)

Table 3.6: Time-line file for baseline run with detectors on

work results which show that the FINDS algorithm, designed on the basis of a bias failure type sensor model, can identify hardover, null, ramp, scale factor, and increase noise type failures as well. That is, the emulation results presented here can be extrapolated to the case for non-bias type sensor failures based on the relative performance comparison between bias and non-bias type failures obtained with the simulation results [3].

Here, we discuss six emulation runs providing a total failure coverage for the fourteen sensors (six input sensors comprised of body mounted accelerometers and rate gyros; and, eight measurement sensors comprised of MLS, IAS, IMU, and radar altimeter sensors). These six runs are discussed by using the "time-line" [2] output files which contain a "snapshot" of the vehicle state estimates at time instants corresponding to important events such as filter turn-on, failure detection and sensor healing decisions, and radar altimeter turn-on.

3.6.1 MLS Elevation Failure

Time-line file given in Table 3.7 shows the results for the first emulation run in which an MLS elevation bias failure is injected into the flight data at 80.65 seconds. The injected bias failure level is 0.18° which corresponds to a 3-sigma failure level with respect to the standard deviation of the MLS elevation measurement noise (see Table 3.2). As can be seen from the time-line in Table 3.7, this bias failure in the second

replication of MLS elevation measurement gets detected at 80.8 seconds yielding a "time-to-detect" figure of 0.15 seconds. As the aircraft state and normal operating bias estimates at 80.65 and 80.8 seconds show, the effects of the failure on the no-fail filter are minimal since the failure is quickly detected in three samples. We also note that this sensor failure takes place in the first segment of the flight (refer to Section 3.4 for the definition of the flight segments) during which the vehicle altitude decreases at a constant rate.

The time-line in Table 3.7 also shows a yaw attitude false alarm at 136.85 seconds which heals itself after 3 seconds. This false alarm is caused mainly by the large inaccuracy in the yaw attitude sensors near the end of the second flight segment during which the aircraft is maneuvering to align itself with the runway as seen in Figure 2.9 in Chapter 2. Since this false alarm is not encountered during the second baseline run with no failures described in the previous section, we can infer that the reinitialization effects of the detected elevation sensor failure is a secondary reason for the false alarm. Table 3.7 shows that the emulation run ends at 298 seconds, after the radar altimeter turn-on at 266.2 seconds.

3.6.2 IMU Yaw, MLS Azimuth and Range Failures

The second time-line file depicted in Table 3.8 show the results for an emulation run in which a sequence of yaw attitude,

```
TIME = 0.05 s.        EVENT : MLS Coverage Begins / Filter Turn On

N-F FILTER STATES :
-1.4403E+04 -4.2300E+03 -7.3396E+02  7.6505E+01  3.7186E+01  3.9929E+00
 3.5800E+00  2.5800E+00  3.1760E+01  0.0000E+00 -1.0302E+01
BIAS FILTER ESTIMATES :
 0.0000E+00  0.0000E+00  0.0000E+00  0.0000E+00  0.0000E+00  0.0000E+00


TIME = 80.65 s.       EVENT : MLS Elevation (Repl. 2) Failure Injected

N-F FILTER STATES :
-1.1846E+04 -1.8944E+03 -4.5291E+02  5.3287E+01  3.3561E+01  3.7722E+00
-7.0555E-02 -6.7442E-01 -3.2063E+02  2.5290E+00 -1.0263E+01
BIAS FILTER ESTIMATES :
-1.8195E-01  5.6236E-02  7.3347E-02 -2.7314E-01 -2.2322E-01  1.3649E-01


TIME = 80.80 s.       EVENT : MLS Elevation (Repl. 2) Failure Detected

N-F FILTER STATES :
-1.1835E+04 -1.8876E+03 -4.5254E+02  5.3253E+01  3.3573E+01  3.8070E+00
 1.5867E-02 -6.7740E-01 -3.2057E+02  2.5533E+00 -1.0300E+01
BIAS FILTER ESTIMATES :
-1.8226E-01  5.6000E-02  7.3800E-02 -2.7314E-01 -2.2322E-01  1.3651E-01


TIME = 136.85 s.      EVENT : Yaw Rate Gyro (Repl. 1) False Alarm

N-F FILTER STATES :
-8.8486E+03 -1.0031E+02 -4.2531E+02  5.9212E+01  2.2479E+01  6.8632E-01
-1.1210E+01  4.9053E+00 -3.3802E+02  6.8303E+00 -1.6195E+01
BIAS FILTER ESTIMATES :
-1.7322E-01  5.9489E-02  6.9669E-02 -2.6855E-01 -2.2470E-01  1.3763E-01


TIME = 139.85 s.      EVENT : Yaw Rate Gyro (Repl. 1) Healed

N-F FILTER STATES :
-8.6659E+03 -4.5426E+01 -4.2637E+02  6.2443E+01  1.6323E+01 -8.0620E-01
-8.8017E+00  3.8177E+00 -3.4441E+02  6.7322E+00 -1.6105E+01
BIAS FILTER ESTIMATES :
-1.7703E-01  5.9017E-02  6.9685E-02 -2.6820E-01 -2.2500E-01  3.0039E-01


TIME = 266.20 s.      EVENT : Radar Altimeter Turn On

N-F FILTER STATES :
-2.5090E+02  3.6452E+00 -3.0449E+01  6.5344E+01  2.6616E-01  3.1512E+00
 2.7464E+00  1.0995E+00 -3.5859E+02 -1.3578E+00 -5.5306E+00
BIAS FILTER ESTIMATES :
-1.8615E-01  5.9363E-02  7.4031E-02 -2.6348E-01 -2.2673E-01 -8.8105E-03



TIME = 298.05 s.      EVENT : End Of Emulation Run

N-F FILTER STATES :
 1.9400E+03 -4.5641E+01 -1.2560E+02  7.5971E+01 -4.6302E+00 -6.8635E+00
 1.9692E-01  9.5383E+00 -3.5723E+02 -1.5177E+00 -5.0753E+00
BIAS FILTER ESTIMATES :
-1.8563E-01  6.3363E-02  1.4139E-01 -2.6298E-01 -2.2690E-01 -8.9562E-03
```

Table 3.7: Time-line file for MLS elevation failure

MLS azimuth and range bias failures are injected into the flight data. In this run, the second replication of the yaw attitude sensor fails at 66.7 seconds with a bias level of 4.0° which corresponds to a 10-sigma failure compared to the yaw attitude sensor noise standard deviation used by the no-fail filter (see Table 3.2). This failure is detected at 66.9 seconds yielding a time-to-detect of 0.2 seconds. The estimated failure level is 2.14° which indicates a small percentage error in the failure level estimate since the yaw attitude measurement is approximately 109 degrees. Due to the fast detection of the failure, there is no significant impact on the no-fail filter estimates.

The time-line in Table 3.8 also shows that the first replication of the MLS azimuth sensor fails at 110.65 seconds, at the beginning of the second flight segment corresponding to the aircraft runway alignment maneuver during which the time rate of change in the azimuth sensor starts gets smaller. The injected bias failure level of 0.18 degrees corresponds to a 3-sigma failure with respect to the MLS azimuth sensor noise parameter used by the no-fail filter. This azimuth failure is detected in 0.4 seconds with a failure level estimate of 0.183 degrees. Again, there is no discernible effect of the failure on the no-fail filter estimates.

The final sensor failure depicted in Table 3.8 is the bias failure in the second replication of the MLS range sensor at 221.95 seconds. At this instant, the aircraft is in the middle

```
TIME = 0.05 s.        EVENT : MLS Coverage Begins / Filter Turn On

N-F FILTER STATES :
-1.4403E+04 -4.2300E+03 -7.3396E+02  7.6505E+01  3.7186E+01  3.9929E+00
 3.5800E+00  2.5800E+00  3.1760E+01  0.0000E+00 -1.0302E+01
BIAS FILTER ESTIMATES :
 0.0000E+00  0.0000E+00  0.0000E+00  0.0000E+00  0.0000E+00  0.0000E+00


TIME = 66.70 s.       EVENT : IMU Yaw (Repl. 2) Failure Injected

N-F FILTER STATES :
-1.2598E+04 -2.3690E+03 -5.0579E+02  5.5228E+01  3.4395E+01  3.0888E+00
 1.4106E+00 -9.3626E-01 -3.2099E+02  1.1067E+00 -7.9917E+00
BIAS FILTER ESTIMATES :
-1.7542E-01  6.5754E-02  7.3244E-02 -2.7288E-01 -2.2283E-01  1.3567E-01


TIME = 66.90 s.       EVENT : IMU Yaw (Repl. 2) Failure Detected

N-F FILTER STATES :
-1.2584E+04 -2.3604E+03 -5.0503E+02  5.5195E+01  3.4359E+01  3.2962E+00
 1.1384E+00 -1.0025E+00 -3.2091E+02  1.1018E+00 -7.9819E+00
BIAS FILTER ESTIMATES :
-1.7498E-01  6.5781E-02  7.3303E-02 -2.7290E-01 -2.2286E-01  1.3517E-01


TIME = 110.65 s.      EVENT : MLS Azimuth (Repl. 1) Failure Injected

N-F FILTER STATES :
-1.0283E+04 -9.3868E+02 -4.3447E+02  5.4272E+01  3.3478E+01 -8.1559E-02
 5.5471E-01  1.3930E+00 -3.2196E+02  5.7069E+00 -1.4775E+01
BIAS FILTER ESTIMATES :
-1.5636E-01  6.4968E-02  7.2387E-02 -2.7198E-01 -2.2230E-01  1.3839E-01


TIME = 111.05 s.      EVENT : MLS Azimuth (Repl. 1) Failure Detected

N-F FILTER STATES :
-1.0258E+04 -9.2529E+02 -4.3437E+02  5.4513E+01  3.3293E+01  2.4125E-01
-4.0756E-02  1.3827E+00 -3.2192E+02  5.7876E+00 -1.4886E+01
BIAS FILTER ESTIMATES :
-1.5623E-01  6.6810E-02  7.2353E-02 -2.7193E-01 -2.2230E-01  1.3839E-01


TIME = 221.95 s.      EVENT : MLS Range (Repl. 2) Failure Injected

N-F FILTER STATES :
-3.1664E+03  3.5177E+00 -2.1399E+02  6.7880E+01  5.6299E-01  4.0661E+00
-1.2385E+00 -3.7735E+00 -3.5416E+02 -5.0399E-01 -6.9357E+00
BIAS FILTER ESTIMATES :
-1.8458E-01  5.9651E-02  7.3423E-02 -2.6403E-01 -2.2703E-01  1.3394E-01
```

Table 3.8: Time-line file for IMU yaw, MLS azimuth and range failures

```
TIME = 222.20 s.      EVENT : MLS Range (Repl. 2) Failure Detected

N-F FILTER STATES :
-3.1468E+03  3.6726E+00 -2.1272E+02  6.7945E+01  3.6251E-01  4.3395E+00
-2.4651E+00 -4.0805E+00 -3.5400E+02 -5.2271E-01 -6.9102E+00
BIAS FILTER ESTIMATES :
-1.8458E-01  5.9542E-02  7.3401E-02 -2.6403E-01 -2.2704E-01  1.3395E-01


TIME = 266.15 s.      EVENT : Radar Altimeter Turn On

N-F FILTER STATES :
-2.5071E+02  3.8884E+00 -3.0400E+01  6.5390E+01  3.7189E-01  3.1198E+00
 2.9754E+00  1.0583E+00 -3.5850E+02 -1.3453E+00 -5.5516E+00
BIAS FILTER ESTIMATES :
-1.8007E-01  6.4311E-02  7.4080E-02 -2.6409E-01 -2.2708E-01  1.3490E-01


TIME = 298.05 s.      EVENT : End Of Emulation Run

N-F FILTER STATES :
 1.9412E+03 -4.5400E+01 -1.2557E+02  7.6030E+01 -4.5117E+00 -6.8588E+00
 3.3815E-01  9.3794E+00 -3.5695E+02 -1.5282E+00 -5.0570E+00
BIAS FILTER ESTIMATES :
-1.7243E-01  6.7891E-02  1.4573E-01 -2.6335E-01 -2.2665E-01  1.3544E-01
```

Table 3.8: Time-line file for IMU yaw, MLS azimuth and range failures (continued)

of the third flight segment, approximately 3200 meters from the range antenna on the runway, and at an altitude of 215 meters. The injected bias failure level of 40 meters corresponds to a 5-sigma failure with respect to the MLS range sensor noise parameter value used by the no-fail filter (Table 3.2). This failure is detected in 0.25 seconds with an estimated failure level of 44.2 meters. The only change in the vehicle state estimates seen in the time-line is in the roll attitude which is caused by a small roll maneuver during 221-222 seconds during which the roll rate gyro is approximately -4 deg/s. The emulation run depicted in Table 3.8 ends after the radar altimeter turn-on at 266.15 seconds.

3.6.3 IAS, Roll Rate and Lateral Accelerometer Failures

Table 3.9 depicts the time-line file corresponding to an emulation run in which a sequence of IAS, roll rate gyro and lateral accelerometer bias failures are injected into the flight data. The first failure is in the IAS sensor at 55.9 seconds. The injected failure level of 9 m/s corresponds to a 6-sigma failure with respect to the IAS noise parameter value used by the no-fail filter (Table 3.2). This failure is detected at 56.1 seconds with a failure level estimate of 9.39 m/s. Since the failure is detected in a relatively short period of 0.2 seconds, there is no significant impact of the failure on the vehicle state estimates. The minor change in the longitudinal accelero-

meter bias estimate could be attributed either to the IAS failure or to the normal transients associated with this bias estimate (Figure 3.8).

At 140.3 seconds, a roll rate gyro failure of 0.9 deg/s is introduced in this run, just after the completion of the runway alignment maneuver. The failure level of 0.9 deg/s corresponds to a 3-sigma failure level with respect to the empirical error statistics given in Table 2.1 (Absolute value of sample mean plus sample standard deviation is approximately 0.3 deg/s for the roll rate gyro). The reason for comparing the input failure levels to the empirical statistics is that the normal operating biases for these sensors are estimated by the no-fail filter. This roll rate gyro failure is detected at 140.85 seconds resulting in a relatively long "time-to-detect" figure of 0.55 seconds. The estimated failure level is approximately 1.4 degrees. As expected, the roll rate gyro failure affects the roll attitude state estimate. There is no such effect on the roll rate gyro bias estimate since this estimate has already converged to its steady state value with a correspondingly small covariance.

The final sensor failure in this run is a lateral accelerometer bias failure of 1.27 m/s^2 at 241 seconds during the landing maneuver flight segment. This failure level corresponds to a 9-sigma failure with respect to the empirical error statistics given in Table 2.1. This failure is detected at 246.4 seconds resulting in a relatively high time-to-detect figure of 5.4

```
TIME = 0.05 s.          EVENT : MLS Coverage Begins / Filter Turn On

N-F FILTER STATES :
-1.4403E+04 -4.2300E+03 -7.3396E+02  7.6505E+01  3.7186E+01  3.9929E+00
 3.5800E+00  2.5800E+00  3.1760E+01  0.0000E+00 -1.0302E+01
BIAS FILTER ESTIMATES :
 0.0000E+00  0.0000E+00  0.0000E+00  0.0000E+00  0.0000E+00  0.0000E+00


TIME = 55.90 s.         EVENT : IAS (Repl. 1) Failure Injected

N-F FILTER STATES :
-1.3202E+04 -2.7458E+03 -5.4476E+02  5.7642E+01  3.4873E+01  4.6800E+00
 3.9162E-01 -2.2503E+00 -3.2150E+02  1.0622E+00 -7.9490E+00
BIAS FILTER ESTIMATES :
-1.5737E-01  8.2514E-02  6.8216E-02 -2.7176E-01 -2.2298E-01  1.3480E-01


TIME = 56.10 ss.        EVENT : IAS (Repl. 1) Failure Detected

N-F FILTER STATES :
-1.3188E+04 -2.7364E+03 -5.4353E+02  5.7659E+01  3.4944E+01  4.7724E+00
 3.8149E-01 -2.0712E+00 -3.2154E+02  1.0602E+00 -7.9534E+00
BIAS FILTER ESTIMATES :
-1.6119E-01  8.1920E-02  6.8178E-02 -2.7179E-01 -2.2287E-01  1.3479E-01


TIME = 140.30 s.        EVENT : Roll Rate Gyro (Repl. 1) Failure Injected

N-F FILTER STATES :
-8.6440E+03 -4.3427E+01 -4.2607E+02  6.2273E+01  1.5041E+01 -3.4536E-01
-9.0896E+00  3.7184E+00 -3.4471E+02  3.6158E+00 -1.1600E+01
BIAS FILTER ESTIMATES :
-1.6975E-01  6.0120E-02  7.0058E-02 -2.6823E-01 -2.2530E-01  1.3696E-01


TIME = 140.85 s.        EVENT : Roll Rate Gyro (Repl. 1) Failure Detected

N-F FILTER STATES :
-8.6068E+03 -3.5242E+01 -4.2632E+02  6.2768E+01  1.4003E+01 -5.5576E-01
-6.7113E+00  4.1704E+00 -3.4491E+02  3.6303E+00 -1.1618E+01
BIAS FILTER ESTIMATES :
-1.6976E-01  5.9972E-02  7.0091E-02 -2.6813E-01 -2.2545E-01  1.3693E-01


TIME = 241.00 s.        EVENT : Lateral Accel. (Repl. 1) Failure Injected

N-F FILTER STATES :
-1.9022E+03  3.9234E+00 -1.3104E+02  6.6541E+01  1.6242E+00  4.1299E+00
-1.0100E+00 -2.2376E+00 -3.5073E+02 -4.1371E-01 -5.6850E+00
BIAS FILTER ESTIMATES :
-1.7117E-01  6.0778E-02  7.2835E-02  1.1215E-01 -2.2612E-01  1.3556E-01
```

Table 3.9: Time-line file for IAS, roll rate gyro and lateral accelerometer failures

```
TIME = 246.40 s.       EVENT : Lateral Accel. (Repl. 1) Failure Detected

N-F FILTER STATES :
-1.5408E+03  1.1281E+01 -1.0940E+02  6.6113E+01  4.1200E+00  4.1311E+00
-1.2592E+00 -1.9185E+00 -3.5180E+02 -5.4173E-01 -5.4847E+00
BIAS FILTER ESTIMATES :
-1.7387E-01  6.8437E-02  7.2797E-02  1.1266E-01 -2.2611E-01  1.3561E-01


TIME = 266.25 s.       EVENT : Radar Altimeter Turn On

N-F FILTER STATES :
-2.4945E+02  4.3244E+00 -3.0388E+01  6.5389E+01  5.9090E-01  3.2155E+00
 2.9520E+00  1.0551E+00 -3.5840E+02 -8.5322E-01 -4.9450E+00
BIAS FILTER ESTIMATES :
-1.6903E-01 -7.2683E-02  7.3143E-02  1.1506E-01 -2.2625E-01  1.3565E-01


TIME = 298.05 s.       EVENT : End Of Emulation Run

N-F FILTER STATES :
 1.9384E+03 -4.6100E+01 -1.2556E+02  7.5846E+01 -4.9852E+00 -6.8486E+00
-4.7219E-01  9.4755E+00 -3.5694E+02 -9.7311E-01 -4.5803E+00
BIAS FILTER ESTIMATES :
-1.7267E-01 -2.9525E-02  1.4260E-01  1.1595E-01 -2.2650E-01  1.3592E-01
```

Table 3.9: Time-line file for IAS, roll rate gyro and lateral accelerometer failures (continued)

seconds. The estimated failure level is 58.25 m/s^2. The large error in the failure level estimate is due to the detection delay. Recalling that the estimation window length for input sensors is 3.0 seconds (Table 3.4), and the previous sensor failure detection (effecting the detector window reinitialization) decision is at 140.85 seconds, the estimated failure level corresponds to a postulated lateral accelerometer failure occurring at 245.85 seconds. As expected, the lateral accelerometer failure affects the vehicle position and velocity estimates in the y-direction. This run ends after radar altimeter turn-on at 266.25 seconds without encountering any false alarms.

As this run illustrates, measurement sensor failures get detected an order of magnitude faster than input sensor failures. This observation is in agreement with the findings of our earlier simulation results. This discrepancy in the time-to-detect figures between the input and measurement sensors is due to the need for input failures to propagate through the no-fail filter dynamics in order to generate identifiable signatures on the residuals.

3.6.4 IMU Roll and Vertical Accelerometer Failures

Table 3.10 gives the results for an emulation run in which a sequence of roll attitude and vertical accelerometer failures are injected into the sensor flight data. As seen from the table, an attitude failure of 1.5 degrees is introduced in the second IMU

roll sensor at 93.25 seconds. This 6-sigma failure (with respect to the filter design parameter) is detected in 0.45 seconds with a failure level of 1.29 degrees. The failure affects the roll attitude estimate which changes from 0.17^{o} to 0.62^{o}. Approximately, half of this change is due to the beginning of the bank maneuver (roll rate gyro is approximately 0.7 deg/s during 93.25-93.7 seconds).

The second failure occurs at 200 seconds in the middle of the landing maneuver. This injected failure of 1.47 m/s^2 is detected in 3.25 seconds with an estimated failure level of 7.67 m/s^2. This failure level corresponds to an 8-sigma failure with respect to the empirical noise statistics given in Table 2.1. The error in the failure level estimate, which is due to the detection delay, is not critical since the FINDS algorithm uses the failure level estimates only indirectly in the covariance increment computation after a failure. As expected, the vertical accelerometer failure has an impact on the vertical velocity estimate. This run ends without encountering any false alarms.

3.6.5 IMU Pitch, Yaw Rate Gyro and Longitudinal Accelerometer Failures

Table 3.11 presents the results for an emulation run where a sequence of IMU pitch attitude, yaw rate gyro, and longitudinal accelerometer failures are injected into the sensor flight data. As seen from the table, the first replication of the IMU pitch

```
TIME = 0.05 s.          EVENT : MLS Coverage Begins / Filter Turn On

N-F FILTER STATES :
-1.4403E+04 -4.2300E+03 -7.3396E+02  7.6505E+01  3.7186E+01  3.9929E+00
 3.5800E+00  2.5800E+00  3.1760E+01  0.0000E+00 -1.0302E+01
BIAS FILTER ESTIMATES :
 0.0000E+00  0.0000E+00  0.0000E+00  0.0000E+00  0.0000E+00  0.0000E+00


TIME = 93.25 s.         EVENT : IMU Roll (Repl. 2) Failure Injected

N-F FILTER STATES :
-1.1190E+04 -1.4872E+03 -4.1303E+02  5.1990E+01  3.2552E+01  8.5998E-01
 1.6729E-01  4.2218E+00 -3.2073E+02  4.5163E+00 -1.3184E+01
BIAS FILTER ESTIMATES :
-1.6833E-01  5.7740E-02  7.3273E-02 -2.7302E-01 -2.2380E-01  1.3755E-01


TIME = 93.70 s.         EVENT : IMU Roll (Repl. 2) Failure Detected

N-F FILTER STATES :
-1.1165E+04 -1.4716E+03 -4.1273E+02  5.1812E+01  3.2463E+01  4.5108E-01
 6.1723E-01  4.5483E+00 -3.2075E+02  4.5730E+00 -1.3264E+01
BIAS FILTER ESTIMATES :
-1.6751E-01  5.8581E-02  7.3304E-02 -2.7321E-01 -2.2385E-01  1.3759E-01


TIME = 200.00 s.        EVENT : Vertical Accel. (Repl. 1) Failure Injected

N-F FILTER STATES :
-4.6365E+03  2.2318E+00 -2.9969E+02  6.7959E+01  5.5326E-01  4.2679E+00
-1.0586E+00 -5.0287E-01 -3.5153E+02 -1.7843E-01 -7.5044E+00
BIAS FILTER ESTIMATES :
-1.8135E-01  5.6697E-02  7.3023E-02 -2.6396E-01 -2.2708E-01  1.3498E-01


TIME = 203.25 s.        EVENT : Vertical Accel. (Repl. 1) Failure Detected

N-F FILTER STATES :
-4.4140E+03  1.3968E+00 -2.7969E+02  6.7373E+01 -3.5945E-02  9.0266E+00
 8.7462E-01 -2.9288E-01 -3.5143E+02 -2.0309E-01 -7.4483E+00
BIAS FILTER ESTIMATES :
-1.8069E-01  5.7171E-02  7.3730E-02 -2.6389E-01 -2.2707E-01  1.3500E-01


TIME = 266.15 s.        EVENT : Radar Altimeter Turn On

N-F FILTER STATES :
-2.5412E+02  3.6643E+00 -3.0442E+01  6.5351E+01  2.9542E-01  3.1775E+00
 2.9595E+00  1.0477E+00 -3.5854E+02 -1.3642E+00 -5.5298E+00
BIAS FILTER ESTIMATES :
-1.7553E-01  6.3732E-02 -2.3427E-02 -2.6393E-01 -2.2707E-01  1.3539E-01



TIME = 298.05 s.        EVENT : End Of Emulation Run

N-F FILTER STATES :
 1.9404E+03 -4.5581E+01 -1.2540E+02  7.6086E+01 -4.5875E+00 -6.8014E+00
 3.0954E-01  9.3699E+00 -3.5697E+02 -1.5127E+00 -5.1100E+00
BIAS FILTER ESTIMATES :
-1.6886E-01  6.7387E-02  4.8259E-02 -2.6303E-01 -2.2659E-01  1.3562E-01
```

Table 3.10: Time-line file for IMU roll and vertical accelerometer failures

attitude fails at 77.85 seconds with a failure level of 2 degrees, which corresponds to a 4-sigma failure level with respect to the no-fail filter design value. This failure is detected at 78.1 seconds, resulting in a time-to-detect figure of 0.25 seconds with an estimated failure level of 1.85 degrees. The time-line also shows that the injected pitch attitude failure induces a false alarm in the pitch rate sensor at 78 seconds which is healed at 81.1 seconds. This is mainly due to the close dynamic coupling between the pitch attitude and pitch rate sensors.

The yaw rate gyro failure of 1 deg/s injected at 152.45 seconds in this run is detected within 2.15 seconds with an estimated failure level of 1.64 deg/s. This failure corresponds to a 7-sigma failure with respect to the empirical noise statistics for the yaw rate gyro. The time-to-detect figure is quite reasonable in light of the large yaw attitude inaccuracy during this time frame (see Figure 2.9).

In the middle of the third flight segment at 221.85 seconds, the longitudinal accelerometer fails with a level of 1.47 m/s^2, which is a 6-sigma failure with respect to the empirical noise statistics for this sensor shown in Table 2.1. This failure is detected in 5.2 seconds with an estimated failure level of 9.09 m/s^2. Again, the large error in the failure level estimate is due to the detection delay for this input sensor.

```
TIME = 0.05 s.          EVENT : MLS Coverage Begins / Filter Turn On

N-F FILTER STATES :
-1.4403E+04 -4.2300E+03 -7.3396E+02  7.6505E+01  3.7186E+01  3.9929E+00
 3.5800E+00  2.5800E+00  3.1760E+01  0.0000E+00 -1.0302E+01
BIAS FILTER ESTIMATES :
 0.0000E+00  0.0000E+00  0.0000E+00  0.0000E+00  0.0000E+00  0.0000E+00


TIME = 77.85 s.         EVENT : IMU Pitch (Repl. 1) Failure Injected

N-F FILTER STATES :
-1.1994E+04 -1.9862E+03 -4.6421E+02  5.3795E+01  3.3972E+01  4.5600E+00
 5.7110E-01 -5.2541E-01 -3.2075E+02  2.1858E+00 -9.7328E+00
BIAS FILTER ESTIMATES :
-1.8377E-01  5.5951E-02  7.3476E-02 -2.7305E-01 -2.2309E-01  1.3628E-01


TIME = 78.00 s.         EVENT : Pitch Rate Gyro (Repl. 1) False Alarm

N-F FILTER STATES :
-1.1983E+04 -1.9795E+03 -4.6331E+02  5.3741E+01  3.3940E+01  4.4822E+00
 5.9257E-01 -4.0480E-01 -3.2074E+02  2.2042E+00 -9.7617E+00
BIAS FILTER ESTIMATES :
-1.8400E-01  5.5865E-02  7.3505E-02 -2.7305E-01 -2.2324E-01  1.3629E-01


TIME = 78.10 s.         EVENT : IMU Pitch (Repl. 1) Failure Detected

N-F FILTER STATES :
-1.1978E+04 -1.9762E+03 -4.6288E+02  5.3638E+01  3.3868E+01  4.4442E+00
 5.7198E-01  3.1011E-01 -3.2073E+02  2.2205E+00 -9.7849E+00
BIAS FILTER ESTIMATES :
-1.8405E-01  5.5907E-02  7.3522E-02 -2.7305E-01 -2.8522E-02  1.3630E-01


TIME = 81.10 s.         EVENT : Pitch Rate Gyro (Repl. 1) Healed

N-F FILTER STATES :
-1.1819E+04 -1.8776E+03 -4.5098E+02  5.3184E+01  3.3566E+01  3.9432E+00
 2.9762E-01 -5.6401E-01 -3.2052E+02  2.5962E+00 -1.0365E+01
BIAS FILTER ESTIMATES :
-1.8299E-01  5.5255E-02  7.3387E-02 -2.7303E-01  4.5969E-02  1.3643E-01


TIME = 152.45 s.        EVENT : Yaw Rate Gyro (Repl. 1) Failure Injected

N-F FILTER STATES :
-7.8414E+03  1.4044E+01 -4.3098E+02  6.7705E+01 -2.7287E+00 -6.6918E-01
 1.4832E+00  6.2148E+00 -3.5726E+02  2.5000E+00 -1.1098E+01
BIAS FILTER ESTIMATES :
-2.0736E-01  5.4184E-02  7.0463E-02 -2.6820E-01  7.3147E-02  1.3538E-01
```

Table 3.11 Time-line file for IMU pitch, yaw rate gyro and longitudinal accelerometer failures

```
TIME = 154.50 s.       EVENT : Yaw Rate Gyro (Repl. 1) Failure Detected

N-F FILTER STATES :
-7.7030E+03  6.2717E+00 -4.3446E+02  6.7538E+01 -2.5927E+00 -1.6868E+00
 2.8304E+00  3.5430E+00 -3.5408E+02  1.8105E+00 -1.0257E+01
BIAS FILTER ESTIMATES :
-2.0967E-01  5.2802E-02  7.0784E-02 -2.6798E-01  7.2100E-02  1.3577E-01


TIME = 221.85 s.       EVENT : Longit. Accel. (Repl. 1) Failure Injected

N-F FILTER STATES :
-3.1731E+03  2.8149E+00 -2.1431E+02  6.7869E+01  5.2323E-01  4.0283E+00
-9.3938E-01 -3.7728E+00 -3.5433E+02 -4.7816E-01 -6.9633E+00
BIAS FILTER ESTIMATES :
-2.1019E-01  5.3670E-02  7.1981E-02 -2.6468E-01  7.5190E-02 -1.3421E-02


TIME = 227.05 s.       EVENT : Longit. Accel. (Repl. 1) Failure Detected

N-F FILTER STATES :
-2.8129E+03  1.3076E+00 -1.8603E+02  7.3313E+01 -1.0360E+00  4.5700E+00
-2.8180E+00 -1.3174E+00 -3.5225E+02 -5.2164E-01 -6.8698E+00
BIAS FILTER ESTIMATES :
-1.9763E-01  5.4197E-02  7.1934E-02 -2.6470E-01  7.4816E-02 -1.2511E-02


TIME = 266.20 s.       EVENT : Radar Altimeter Turn On

N-F FILTER STATES :
-2.5132E+02  3.7283E+00 -3.0446E+01  6.5050E+01  3.0628E-01  3.1602E+00
 2.7395E+00  1.4594E+00 -3.5853E+02 -1.3540E+00 -5.5409E+00
BIAS FILTER ESTIMATES :
 9.3235E-02  5.4547E-02  7.3689E-02 -2.6460E-01  7.6029E-02 -1.0589E-02


TIME = 298.05 s.       EVENT : End Of Emulation Run

N-F FILTER STATES :
 1.9386E+03 -4.5678E+01 -1.2568E+02  7.5525E+01 -4.6310E+00 -6.8717E+00
 2.0780E-01  1.0263E+01 -3.5718E+02 -1.5202E+00 -5.0828E+00
BIAS FILTER ESTIMATES :
 5.5197E-02  5.7721E-02  1.2080E-01 -2.6399E-01  7.6797E-02 -1.0081E-02
```

Table 3.11 Time-line file for IMU pitch, yaw rate gyro and longitudinal accelerometer failures (continued)

3.6.6 Pitch Rate and Radar Altimeter Failures

Table 3.12 summarizes the results for an emulation run where a sequence of pitch rate gyro and radar altimeter failures are injected into the flight data. The pitch rate gyro fails at 179.95 seconds with a failure level of 1 deg/s, which corresponds to approximately a 4-sigma failure with respect to the empirical error statistics for this sensor. This failure is detected in 0.55 seconds with an estimated failure level of 0.36 deg/s. There are no significant effects on the filter estimates due to the pitch rate gyro failure.

In this run, a false alarm in the longitudinal accelerometer is encountered at 255.55 seconds which is healed in 3 seconds. The radar altimeter is turned on at 266.2 seconds, and a failure level of 6 meters is injected into the second replication of the radar altimeter at 270.25 seconds. This 6-sigma failure (with respect to the filter noise design value) is detected in 0.6 seconds with an estimated failure level of 5.68 meters. This run ends after a pitch attitude false alarm at 282.75 seconds; this can be attributed to the inaccuracies in the MLS sensors during the touch-and-go maneuver when the aircraft is beyond the MLS azimuth and range antennas.

The six emulation runs described above give a complete failure coverage for all of the 14 sensors. The results are summarized in Table 3.13 which gives, for each sensor type, the injected bias failure level, the estimated failure magnitude, and time-to-detect figure.

```
TIME = 0.05 s.          EVENT : MLS Coverage Begins / Filter Turn On

N-F FILTER STATES :
-1.4403E+04 -4.2300E+03 -7.3396E+02  7.6505E+01  3.7186E+01  3.9929E+00
 3.5800E+00  2.5800E+00  3.1760E+01  0.0000E+00 -1.0302E+01
BIAS FILTER ESTIMATES :
 0.0000E+00  0.0000E+00  0.0000E+00  0.0000E+00  0.0000E+00  0.0000E+00


TIME = 178.95 s.        EVENT : Pitch Rate Gyro (Repl. 1) Failure Injected

N-F FILTER STATES :
-6.0735E+03 -2.7737E+00 -3.9040E+02  6.8129E+01  3.2448E-01  3.4742E+00
 2.0920E+00 -1.1813E+00 -3.5170E+02 -2.1831E-01 -7.6157E+00
BIAS FILTER ESTIMATES :
-1.9346E-01  5.2832E-02  7.2170E-02 -2.6451E-01 -2.2829E-01  1.3483E-01


TIME = 179.50 s.        EVENT : Pitch Rate Gyro (Repl. 1) Failure Detected

N-F FILTER STATES :
-6.0332E+03 -2.8415E+00 -3.8833E+02  6.8158E+01  5.2239E-01  3.4849E+00
 2.5160E+00 -9.6758E-01 -3.5188E+02 -2.2410E-01 -7.6038E+00
BIAS FILTER ESTIMATES :
-1.9267E-01  5.2825E-02  7.2189E-02 -2.6446E-01 -2.2828E-01  1.3482E-01


TIME = 255.55 s.        EVENT : Longit. Accel. (Repl. 1) False Alarm

N-F FILTER STATES :
-9.3319E+02  4.7232E+00 -7.1694E+01  6.6946E+01  1.5875E+00  4.4737E+00
 1.0420E-01 -2.0788E+00 -3.5357E+02 -1.2424E+00 -5.7568E+00
BIAS FILTER ESTIMATES :
-1.9425E-01  6.0951E-02  7.3297E-02 -2.6378E-01  7.6561E-02  1.3529E-01


TIME = 258.55 s.        EVENT : Longit. Accel. (Repl. 1) Healed

N-F FILTER STATES :
-7.3773E+02  6.1712E+00 -5.7900E+01  6.6163E+01 -2.6692E-01  5.3613E+00
-1.1904E+00 -6.5330E-01 -3.5535E+02 -1.2970E+00 -5.6664E+00
BIAS FILTER ESTIMATES :
 3.8362E-01  6.1708E-02  7.3526E-02 -2.6383E-01  7.6756E-02  1.3528E-01


TIME = 266.20 s.        EVENT : Radar Altimeter Turn On

N-F FILTER STATES :
-2.5255E+02  3.6614E+00 -3.0473E+01  6.4503E+01  2.8403E-01  3.1627E+00
 2.7496E+00  1.2728E+00 -3.5847E+02 -1.3725E+00 -5.5160E+00
BIAS FILTER ESTIMATES :
 2.4785E-01  6.0865E-02  7.3652E-02 -2.6386E-01  7.8685E-02  1.3527E-01
```

Table 3.12: Time-line file for pitch rate gyro and radar altimeter failures

```
TIME = 270.25 s.      EVENT : Radar Altimeter (Repl. 2) Failure Injected

N-F FILTER STATES :
 2.0413E+01  4.3853E+00 -1.9686E+01  6.7304E+01  4.3931E-01  6.1135E+00
 3.3030E+00 -6.5059E-01 -3.5895E+02 -1.3488E+00 -5.6393E+00
BIAS FILTER ESTIMATES :
 3.3523E-02  5.7245E-02 -3.0072E-01 -2.6384E-01  7.8943E-02  1.3529E-01


TIME = 270.85 s.      EVENT : Radar Altimeter (Repl. 2) failure Detected

N-F FILTER STATES :
 6.3420E+01  5.0422E+00 -1.6824E+01  6.7347E+01  4.1358E-01  6.4742E+00
 2.8997E+00 -5.8930E-01 -3.5903E+02 -1.3691E+00 -5.5762E+00
BIAS FILTER ESTIMATES :
 7.8674E-03  5.8205E-02 -2.0024E-01 -2.6383E-01  7.9004E-02  1.3529E-01


TIME = 282.75 s.      EVENT : IMU Pitch (Repl. 1) False Alarm

N-F FILTER STATES :
 8.3985E+02  8.1929E+00 -1.4886E+01  6.8282E+01 -5.1800E-02 -6.2402E+00
 1.3723E+00  1.1889E+01 -3.5421E+02 -1.4854E+00 -5.1867E+00
BIAS FILTER ESTIMATES :
 6.6415E-02  6.5507E-02  2.1783E-01 -2.6375E-01  8.1592E-02  1.3552E-01


TIME = 298.05 s.      EVENT : End Of Emulation Run

N-F FILTER STATES :
 1.9396E+03 -4.5634E+01 -1.2551E+02  7.5824E+01 -4.6127E+00 -6.9288E+00
 2.7582E-01  9.9770E+00 -3.5697E+02 -1.5301E+00 -5.0228E+00
BIAS FILTER ESTIMATES :
 4.6459E-02  6.7018E-02  1.2472E-01 -2.6345E-01  8.1284E-02  1.3554E-01
```

Table 3.12: Time-line file for pitch rate gyro and radar altimeter failures (continued)

As discussed in the individual failure runs, the relatively high estimated failure levels for accelerometers are due to the comparatively long detection delays for these instruments. The reason for the high time-to-detect figures for accelerometer failures is the need for such failures to propagate through the no-fail filter dynamics in order to generate indentifiable signatures on the MLS measurement residuals. However, these high accelerometer failure level estimates do not have an unfavorable impact on the FINDS algorithm since failure level estimates are used only in incrementing the no-fail filter covariance after the identification of a failure.

Run No.	Sensor Type	Detection Time (s)	Injected Fail. Lev	Estim. Fail. Lev	Units
1	MLS Elevation	0.15	0.18	0.107	deg
2	IMU Yaw	0.20	4.00	2.14	deg
2	MLS Azimuth	0.40	0.18	0.183	deg
2	MLS Range	0.25	40.0	44.2	m
3	IAS	0.20	9.00	9.391	m/s
3	Roll Rate Gyro	0.55	0.90	1.40	deg/s
3	Lateral Accel.	5.40	1.275	58.25	m/s/s
4	IMU Roll	0.45	1.50	1.285	deg
4	Vertical Accel.	3.25	1.471	7.675	m/s/s
5	IMU Pitch	0.25	2.00	1.852	deg
5	Yaw Rate Gyro	2.05	1.00	1.635	deg/s
5	Longit. Accel.	5.20	1.471	9.092	m/s/s
6	Pitch Rate Gyro	0.55	1.00	0.356	deg/s
6	Radar Altimeter	0.60	6.00	5.678	m

Table 3.13: Bias failure performance summary

4 CONCLUSIONS AND RECOMMENDATIONS

We have presented an analysis of the FINDS algorithm performance using flight recorded sensor data from the NASA ATOPS B-737 aircraft. Results indicate the exceptional vehicle state and sensor bias estimation performance for the no-fail filter employed in the FINDS algorithm. Results also show an excellent failure detection and isolation performance with detection speed (in agreement with our earlier simulation studies) considerably faster for no-fail filter measurement sensors such as MLS than for input sensors such as accelerometers. Finally, emulation results show a general improvement, both in false alarm and detection speed performance, resulting from the modifications which we have made in the current study to the detector and decision algorithms in FINDS. Based on our analysis, we recommend that the FINDS algorithm be modified in order to run within the memory and speed constraints of the TSRV flight computers

REFERENCES

[1] Caglayan, A.K. and Lancraft, R.E., "An Aircraft Sensor Fault Tolerant System", NASA CR-165876, April 1982.

[2] Lancraft, R.E. and Caglayan, A.K., "FINDS: A Fault Inferring Nonlinear Detection System: User's Guide", NASA CR-172199, September 1983.

[3] Caglayan, A.K. and Lancraft, R.E., "A Fault Tolerant System for an Integrated Avionics Sensor Configuration.", NASA CR-3834, September 1984.

[4] Duff, W.G. and Guarino, C.R., "Refinement and Validation of two Digital Microwave Landing System (MLS) Theoretical Models", NASA CR-132713, August 1975.

[5] Anderson, T.W., An Introduction to Multivariate Statistical Analysis, John Wiley and Sons, New York, 1958.

1. Report No.	2. Government Accession No.	3. Recipient's Catalog No.
NASA CR-172589		

4. Title and Subtitle	5. Report Date
EVALUATION OF A FAULT TOLERANT SYSTEM FOR AN INTEGRATED AVIONICS SENSOR CONFIGURATION WITH TSRV FLIGHT DATA	June 1985
	6. Performing Organization Code

7. Author(s)	8. Performing Organization Report No.
A. K. Caglayan and P. M. Godiwala	R8502
	10. Work Unit No.

9. Performing Organization Name and Address	11. Contract or Grant No.
Charles River Analytics Inc. 55 Wheeler Street Cambridge, MA 02138	NAS1-17719
	13. Type of Report and Period Covered
12. Sponsoring Agency Name and Address	Contractor Report
National Aeronautics and Space Administration Washington, DC 20546	14. Sponsoring Agency Code

15. Supplementary Notes

Langley Technical Monitor: Frederick R. Morrell
Final Report

16. Abstract

This report presents the performance analysis results of a fault inferring nonlinear detection system (FINDS) using sensor flight data for the NASA ATOPS B-737 aircraft in a Microwave Landing System (MLS) environment. First, a statistical analysis of the flight recorded sensor data was made in order to determine the characteristics of sensor inaccuracies. Next, modifications were made to the detection and decision functions in the FINDS algorithm in order to improve false alarm and failure detection performance under real modelling errors present in the flight data. Finally, the failure detection and false alarm performance of the FINDS algorithm were analyzed by injecting bias failures into fourteen sensor outputs over six repetetive runs of the five minute flight data. In general, the detection speed, failure level estimation, and false alarm performance showed a marked improvement over the previously reported simulation runs. In agreement with earlier results, detection speed was faster for filter measurement sensors such as MLS than for filter input sensors such as flight control accelerometers.

17. Key Words (Suggested by Author(s))	18. Distribution Statement
Fault tolerant systems, Integrated avionics, Sensor failure detection	Unclassified - Unlimited

19. Security Classif. (of this report)	20. Security Classif. (of this page)	21. No. of Pages	22. Price
Unclassified	Unclassified	87	